arXiv:1703.10937v1 [cond-mat.str-el] 31 Mar 2017

Towards a complete classification of fermionic symmetry protected topological phases in 3D and a general group supercohomology theory

Qing-Rui Wang[1] and Zheng-Cheng Gu[1]

[1] *Department of Physics, The Chinese University of Hong Kong, Shatin, New Territories, Hong Kong, China*

(Dated: April 3, 2017)

Classification and construction of symmetry protected topological (SPT) phases in interacting boson and fermion systems have become a fascinating theoretical direction in recent years. It has been shown that the (generalized) group cohomology theory or cobordism theory can give rise to a complete classification of SPT phases in interacting boson/spin systems. Nevertheless, the construction and classification of SPT phases in interacting fermion systems are much more complicated, especially in 3D. In this work, we revisit this problem based on the equivalent class of fermionic symmetric local unitary (FSLU) transformations. We construct very general fixed point SPT wavefunctions for interacting fermion systems. We naturally reproduce the partial classifications given by special group super-cohomology theory, and we show that with an additional $\tilde{B}H^2(G_b, \mathbb{Z}_2)$ (the so-called obstruction free subgroup of $H^2(G_b, \mathbb{Z}_2)$) structure, a complete classification of SPT phases for three-dimensional interacting fermion systems with a total symmetry group $G_f = G_b \times \mathbb{Z}_2^f$ can be obtained for unitary symmetry group G_b. We also discuss the procedure of deriving a general group super-cohomology theory in arbitrary dimensions.

CONTENTS

I. Introduction 2

II. Fixed point wavefunction of FSPT states 4

III. Constructions and classifications for FSPT states in 2D 6
A. Discrete spin structure and Kasteleyn orientations 7
1. Discrete Stiefel-Whitney homology class w_0 7
2. Kasteleyn orientations and gauge transformations 8
3. Kasteleyn orientations under retriangulations 10
B. Fermionic symmetric local unitary transformations and consistent equations 10
1. Decoration of Kitaev's Majorana chains 10
2. Fermionic pentagon equations 12

IV. Constructions and classifications for FSPT states in 3D 13
A. Discrete spin structure in 3D and local Kasteleyn orientations 13
1. Discrete Stiefel-Whitney homology class w_1 14
2. Local Kasteleyn orientations and gauge transformations 14
3. Local Kasteleyn orientations under retriangulations 16
B. Fermionic symmetric local unitary transformations and consistent equations 17
1. Fermion parity and the obstruction of Kitaev's Majorana chain decoration 17
2. Fermionic symmetric local unitary transformations 19
3. Fermionic hexagon equation 21

V. Conclusions and discussions 25

Acknowledgments 25

A. 2D Pachner moves 25
1. (2-2) moves 25
2. (1-3) moves 27

B. 3D Pachner moves and fermion parity changes 27
1. (2-3) moves 27
2. (1-4) moves 29

C. Abelian group structure of the general group super-cohomology solutions 34
1. Explicit construction of $\theta[n_3, n_3', \tilde{n}_2, \tilde{n}_2']$ 35
2. Solving system of linear equations in $\mathbb{R}/4\mathbb{Z}$ 35

References 37

I. INTRODUCTION

In recent years, a new type of topological order – symmetry protected topological (SPT) order [1–3] has been proposed and intensively studied in interacting boson and fermion systems. 2D and 3D topological insulators (TI) [4, 5] are the simplest examples of SPT phases, which are protected by time reversal and charge conservation symmetries. Although topological insulators were initially proposed and experimentally realized in (almost) non-interacting electron systems, very recent studies have established their existence and stability even in the presence of strong interactions by computing (non-perturbative) quantum anomaly on various manifolds [6]. The first attempt to systematically understand SPT phases in interacting systems was proposed in Ref. 1, which pointed out that the well known Haldane chain [7] is actually an SPT phase! Later, a systematic classification of SPT phases for interacting bosonic systems in arbitrary dimension with an arbitrary global symmetry was achieved by using (generalized) group cohomology theory [2, 3, 8] or cobordism theory [9], which essentially classifies the quantum anomalies associated with the corresponding global symmetries in interacting bosonic systems. In terms of physical picture, it has been further pointed out that by gauging the global symmetry G, different SPT phases can be characterized by different types of braiding statistics of G-flux/flux lines in 2D/3D [10–17]. Moreover, anomalous surface topological order was also proposed as another very powerful way to identify and characterize different 3D SPT phases in interacting boson and fermion systems [18–27].

From the quantum information perspective, (intrinsic) topological phases are gapped quantum states that can be defined and classified by inequivalent class of (finite depth) local unitary (LU) transformations [28], which leads to the novel concept of long range entanglement. However, in contrast to those (intrinsic) topological phases, all SPT phases can be adiabatically connected to a trivial disordered phase or an atomic insulator without symmetry protection. Therefore, SPT phases only contain short-range entanglement and they can be constructed by applying local unitary transformations on a trivial product state. In particular, Ref. 2 and 3 introduced a systematic way to construct fixed point ground state wavefunction for bosonic SPT phases on arbitrary triangulations in arbitrary dimensions. It turns out that such a construction is fairly complete for bosonic SPT phases protected by unitary symmetry group(up to 3D). So far the only known example beyond this construction is the so-called $efmf$ SPT state [18] protected by time reversal symmetry in 3D. Later, it was shown that such an exotic bosonic SPT state can be realized by Walker-Wang model [29, 30].

Nevertheless, the classification and systematic understanding of SPT phases in interacting fermion systems are much more complicated. One obvious way with fruitful results is the study on reduction of the free-fermion classifications [31, 32] under the effect of interactions [33–39]. However, these works miss those fermionic SPT (FSPT) phases that can not be realized in free fermion systems. A slightly generalized way to understand FSPT in interacting fermion systems is to stack some additional bosonic SPT states onto a free fermion SPT state[40]. For example, an arguable fairly complete classification of TI in interacting electron systems [41] can be constructed in such a way. However, there is no natural reason to believe that all FSPT phases in interacting systems can be realized by the above stacking constructions and counter examples can be constructed explicitly. Moreover, it has also been shown that certain bosonic SPT phases will become "trivial" (adiabatically connected to a product state) [40, 42] when embedding into interacting fermion systems. Apparently, the stacking construction can not explain all these subtle issues. Therefore, a systematic understanding and construction of interacting FSPT phases are very desired.

The first attempt to classify interacting FSPT phases in general dimensions was proposed in Ref. 42, where a class of FSPT phases was constructed systematically by generalizing the usual group cohomology theory into the so-called special group super-cohomology theory. However, it turns out that such a construction can not give rise to all FSPT phases (except in 1D, where the obtained classification of FSPT phases perfectly agrees with previous results [43, 44]). On the other hand, quantum anomaly characterized by spin cobordism[45] or invertable spin topological quantum field theory (TQFT)[46–48] suggests a very rich world of FSPT phases, though it is not clear how to construct these FSPT states in an explicit and systematic way.

Alternatively, the idea of gauging fermion parity [37, 49–52] provides us another way to understand FSPT. In 2D, fairly complete classification of FSPT can be obtained in this way, which also agrees with the anomaly classification given by spin cobordism and invertable spin TQFT [45, 46, 48]. It has been shown that the mathematical objects that classify 2D FSPT phases with a total symmetry $G_f = G_b \times \mathbb{Z}_2^f$ can be summarized as three group cohomologies of the symmetry group [48, 50]: $H^1(G_b, \mathbb{Z}_2)$, $BH^2(G_b, \mathbb{Z}_2)$ and $H^3(G_b, U_T(1))$. $H^1(G_b, \mathbb{Z}_2)$ which one-to-one corresponds to the $\mathbb{Z}_2$ subgroups of G_b, classifies FSPT phases with Majorana edge modes. $BH^2(G_b, \mathbb{Z}_2)$, the obstruction free

subgroup of $H^2(G_b,\mathbb{Z}_2)$ is formed by elements $n_2\in H^2(G_b,\mathbb{Z}_2)$ that satisfy $Sq^2(n_2)=0$ in $H^4(G_b,U_T(1))$, where Sq^2 is the Steenrod square $Sq^2: H^d(G_b,\mathbb{Z}_2)\to H^{d+2}(G_b,\mathbb{Z}_2)\subset H^{d+2}[G_b,U_T(1)]$. $H^3(G_b,U_T(1))$ is the well-known classification of bosonic SPT phases. Physically, the $H^1(G_b,\mathbb{Z}_2)$ layer can be constructed by decorating a Majorana chain [53] (which is a 1D invertable fermionic TQFT) onto the domain walls of symmetry group G_b and the $BH^2(G_b,\mathbb{Z}_2)$ layer can be constructed by decorating complex fermion (which is a 0D invertable TQFT) onto the intersection points of G_b-symmetry domain walls. Nevertheless, the decoration scheme could suffer from obstructions and only a subgroup $BH^2(G_b,\mathbb{Z}_2)$ classifies valid and inequivalent 2D FSPT phases. In 3D, a few interesting examples of SPT phases are studied based on Walker-Wang model construction [54], e.g., DIII class topological superconductor [24, 55–57]. However, it is unclear how to construct all FSPT phases by using Walker-Wang model. In fact, it is even unclear how to reproduce all the special group super-cohomology constructions in this way. Very recently, some new interacting FSPT phases beyond special group super-cohomology are formally proposed by using spin TQFT [58]; however, there is still lacking of general principle and lattice model realizations.

In this paper, we would like to propose a general physical principle to obtain all FSPT phases in 3D with total symmetry group $G_f=G_b\times\mathbb{Z}_2^f$, where G_b is the bosonic global symmetry and $\mathbb{Z}_2^f$ is the fermion parity conservation symmetry. In a previous work, it has been shown that in the presence of global symmetry, symmetry enriched topological (SET) phases can be defined and classified by equivalent class of symmetric local unitary (SLU) transformations [59, 60]. In particular, SPT phases can be realized as a special class of SET phases whose bulk excitations are trivial and can be adiabatically connected to a product state in the absence of global symmetry. In Ref. 61, it has been shown that fermionic local unitary (FLU) transformations can be used to define and classify (intrinsic) topological phases for interacting fermion systems. The Fock space structure and fermion parity conservation symmetry of fermion systems can be naturally encoded into FLU transformations. Thus, it is not quite surprising that in the presence of global symmetry, we can just introduce the notion of fermionic symmetric local unitary (FSLU) transformations to define and classify fermionic SET (FSET) phases in interacting fermion systems. Similar to the bosonic case, FSPT phases are special class of FSET phases that have trivial bulk excitations and can be adiabatically connected to a product state in the absence of global symmetry. Technically, we only need to enforce the support dimension of FSLU transformations equal to one to classify FSPT states.

Essentially, the novel concept of FSLU transformation allows us to construct very general fixed point FSPT states of 2D and 3D FSPT phases. Moreover, all these fixed point wavefucntions admit exact solvable parent Hamiltonians consisting of commuting projectors on an arbitrary triangulation with an arbitrary branching structure. We will begin with the 2D case where the discrete spin structure can be implemented by Kasteleyn orientation [62–64] that allows us to decorate Majorana chain onto G_b-symmetry domain walls [65, 66]. Then we will show how to implement the discrete spin structure on a triangulation of 3D (orientable) spin manifold, which is a nontrivial generalization of Kasteleyn orientation. The discrete spin structure allows us to decorate the Majorana chain onto the intersection lines of G_b-symmetry domain walls in a self consistent and topological invariant way. The fundamental mathematical data describing such a decoration scheme belong to $H^2(G_b,\mathbb{Z}_2)$, subjected to an obstructions on $H^4(G_b,\mathbb{Z}_2)$. The obstruction can be understood by the following physical picture: Since Kasteleyn orientation is not always possible for a large loop (the 3D discrete spin structure can be used to construct *local* Kasteleyn orientation of small loops within a tetrahedron), a complex fermion decoration on the intersection points of G_b-symmetry domain walls is typically required and this is only possible when the $H^4(G_b,\mathbb{Z}_2)$ obstruction vanishes. Furthermore, another obstruction on $H^5(G_b,U_T(1))$ will be generated by wavefunction renormalization to finally determine whether the entire decoration scheme of Majoarana chain is valid or not for a fixed point wavefunction in 3D.

The precise mathematical objects that classify 3D FSPT phases with a total symmetry $G_f=G_b\times\mathbb{Z}_2^f$ can also be summarized as three group cohomologies of the symmetry group: $\tilde{B}H^2(G_b,\mathbb{Z}_2)$, $BH^3(G_b,\mathbb{Z}_2)$ and $H^4_{\text{rigid}}(G_b,U_T(1))$. $\tilde{B}H^2(G_b,\mathbb{Z}_2)$, the obstruction free subgroup of $H^2(G_b,\mathbb{Z}_2)$, is formed by elements $\tilde{n}_2\in H^2(G_b,\mathbb{Z}_2)$ that simultaneously satisfy $Sq^2(\tilde{n}_2)=0$ in $H^4(G_b,\mathbb{Z}_2)$ and $\mathcal{O}(\tilde{n}_2)=0$ in $H^5(G_b,U_T(1))$, where $\mathcal{O}$ is some unknown cohomology operation (to the best of our knowledge) that maps $\tilde{n}_2$ satisfying $Sq^2(\tilde{n}_2)=0$ in $H^2(G_b,\mathbb{Z}_2)$ into an element in $H^5(G_b,\mathbb{Z}_8)\subset H^5[G_b,U_T(1)]$. The explicit expression of $\mathcal{O}$ is very complicated and will be computed in a physical way in section IV B. $BH^3(G_b,\mathbb{Z}_2)$, the obstruction free subgroup of $H^3(G_b,\mathbb{Z}_2)$ is formed by elements $n_3\in H^3(G_b,\mathbb{Z}_2)$ that satisfy $Sq^2(n_3)=0$ in $H^4(G_b,U_T(1))$. We note that $BH^3(G_b,\mathbb{Z}_2)$ and $H^4_{\text{rigid}}(G_b,U_T(1))\equiv H^4(G_b,\mathbb{Z}_2)/\Gamma$ were derived in the special group super-cohomology classification. Recall that $H^4(G_b,U_T(1))$ is the well-known classification of bosonic SPT phases and Γ is a normal subgroup of $H^4(G_b,U_T(1))$ generated by $Sq^2(n_2)$, where $n_2\in H^2(G_b,\mathbb{Z}_2)$ and $Sq^2(n_2)$ are viewed as elements of $H^4[G_b,U_T(1)]$. Physically, Γ describes those trivialized bosonic SPT phases when embedded into interacting fermion systems.

Together with several previous works, we conjecture that up to spacial dimension $d_{sp}=3$, FSPT with symmetry $G_f=G_b\times\mathbb{Z}_2^f$ can be classified by the general group super-cohomology class $H_f^{d_{sp}+1}[G_f,U_T(1)]$ defined by the exact sequences summarized in table I. We note that for spacial dimension $d_{sp}>1$, the general group super-cohomology theory will be defined by two short exact sequences. The first short exact sequence can be understood as decoration

d_{sp}	short exact sequence
0	$0 \to H^1[G_b, U_T(1)] \to H^1_f[G_f, U_T(1)] \to \mathbb{Z}_2 \to 0$
1	$0 \to H^2[G_b, U_T(1)] \to H^2_f[G_f, U_T(1)] \to H^1(G_b, \mathbb{Z}_2) \to 0$
2	$0 \to H^3[G_b, U_T(1)] \to \mathcal{H}^3[G_f, U_T(1)] \to BH^2(G_b, \mathbb{Z}_2) \to 0$ $0 \to \mathcal{H}^3[G_f, U_T(1)] \to H^3_f[G_f, U_T(1)] \to H^1(G_b, \mathbb{Z}_2) \to 0$
3	$0 \to H^4_{\text{rigid}}[G_b, U_T(1)] \to \mathcal{H}^4[G_f, U_T(1)] \to BH^3(G_b, \mathbb{Z}_2) \to 0$ $0 \to \mathcal{H}^4[G_f, U_T(1)] \to H^4_f[G_f, U_T(1)] \to \tilde{B}H^2(G_b, \mathbb{Z}_2) \to 0$

TABLE I: Classify FSPT phases up to spacial dimension $d_{sp} = 3$ with symmetry $G_f = G_b \times \mathbb{Z}_2^f$ by using general group super-cohomology class computed from short exact sequences.

of complex fermion onto the intersection points of G_b-symmetry domain walls, which was first derived by the special group super-cohomology theory. The second exact sequence can be understood as decoration of Kitaev's Majorana chain onto the intersection lines of G_b-symmetry domain walls and our construction give rise to a general scheme to compute $\tilde{B}H^{d_{sp}-1}(G_b, \mathbb{Z}_2)$ (the obstruction free subgroup of $H^{d_{sp}-1}(G_b, \mathbb{Z}_2)$) in arbitrary dimensions.

Finally, regarding the completeness of general group super-cohomology classification for 3D FSPT phases, we would like to give some physical arguments here. Although the decoration of complex fermion on the intersection points of G_b-symmetry domain walls and the decoration of Majorana chain on G_b-symmetry domain walls give rise to a complete classification of 2D FSPT phases, it does not necessarily imply this is also true in 3D. In fact, it has been pointed out [8] that the decoration of invertable TQFT on the G_b-symmetry domain walls might also gives rise to new SPT states. For bosonic SPT states, a decoration of the so-called E_8 state on the G_b-symmetry domain walls indeed produces the $efmf$ SPT state beyond group cohomology classification. It was also pointed out that $H^1(G_b, \mathbb{Z})$ classifies these additional bosonic SPT. Since $H^1(G_b, \mathbb{Z})$ is trivial for unitary symmetry group G_b and $H^1(\mathbb{Z}_2^T, \mathbb{Z}) = \mathbb{Z}_2$ for the anti-unitary time reversal symmetry, we understand the reason why $efmf$ state is the only non-trivial route state of bosonic SPT states beyond group cohomology classification with time reversal symmetry. For interacting fermion systems, in principle we can decorate a $p + ip$ state (the root state of 2D fermionic invertable TQFT) onto the G_b-symmetry domain walls. However, since $H^1(G_b, \mathbb{Z})$ is trivial for unitary symmetry group G_b, there will be no new FSPT states with unitary symmetry group G_b. For time reversal symmetry, it is possible to generate new FSPT states in this way, and we will discuss this possibility in our future work.

The rest part of the paper is organized as follows. We will begin with the definition of Hilbert space and the basic structure of fixed point wavefunctions for FSPT states with a total symmetry $G_f = G_b \times \mathbb{Z}_2^f$ in 2D and 3D. In section III A, we will give a brief review for discrete spin structure and Kasteleyn orientation in 2D. In section III B, we will derive the fixed point conditions for FSLU transformations under wavefunction renormalization and re-derive the classifications of 2D FSPT phases. In section IV A, we will discuss how to generalize the discrete spin structure in 3D. In section IV B, we will use the concept of equivalent class of FSLU transformations and wavefunction renormalization to obtain the classifications and constructions of 3D FSPT phases. Finally, there will be conclusions and discussions for possible future directions.

II. FIXED POINT WAVEFUNCTION OF FSPT STATES

Similar to the wave function renormalization scheme for 2D bosonic SET phases, here we will consider quantum state defined on an arbitrary triangulation for 2D and 3D FSPT phases. The triangulation admits a branching structure that can be labelled by a set of local arrows on all links (edges) with no oriented loop for any triangle. Mathematically, the branching structure can be regarded as a discrete version of spin^c structure and can be consistently defined on arbitrary triangulations of orientable manifolds.

Let us begin with the construction of fixed point wavefunction in 2D, and the generalization into 3D will be straightforward. Since any 2D FSPT state can be naturally mapped to a 2D bosonic SET state by gauging the fermion parity symmetry, our construction for fixed point wavefucntions will be greatly inspired by such kind of connections. In particular, an FSPT state with total symmetry $G_f = G_b \times \mathbb{Z}_2^f$ can be mapped to a G_b symmetry enriched toric code model. As a simple example, fixed point wavefucntions and commuting projector parent Hamiltonians on arbitrary trivalent graph (due of a triangulation) with $G_b = \mathbb{Z}_2$ are constructed in Ref. 59. It has also been shown that all these SET states can be obtained by gauging fermion parity from FSPT states with total symmetry $G_f = \mathbb{Z}_2 \times \mathbb{Z}_2^f$.

The building block of bosonic and fermionic degrees of freedom of our 2D FSPT model is shown in Fig. 1. Exactly the same as bosonic SET phase, every vertex i of the space triangulation has a bosonic degrees of freedom labelled by a group element $g_i \in G_b$ (recall that the FSPT phases have a total symmetry $G_f = G_b \times \mathbb{Z}_2^f$). A spinless complex fermion c lives at the center of each triangle/face (see blue ball in Fig. 1), and the fermion occupation number is either

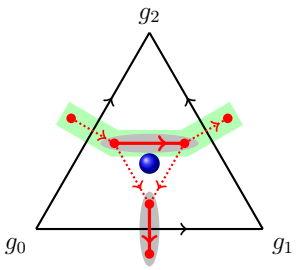

FIG. 1: Fermionic degrees of freedom in a triangle. Red dots represent Majorana fermions at the two sides of each link. Blue ball represents the complex fermion of the special group super-cohomology model at the center of the triangle. Green strip is the decorated Kitaev's Majorana chain on the dual lattice $\mathcal{P}$.

0 or 1. Let $|0\rangle$ be the ground state of no fermions on all triangles, then a generating set of the Fock space is given by $\prod_{(ijk)\in f} c^\dagger_{(ijk)}|0\rangle$, where $f \subset F$ is a subset of all triangles F including the empty set. In addition, each link has two Majorana fermions on its two sides, which is equivalent to a spinless complex fermion a. Similar to the c fermion on each triangle, let $|\tilde{0}\rangle$ be the ground state of no fermions on all links, then a generating set of the Fock space is given by $\prod_{(ij)\in l} a^\dagger_{(ij)}|\tilde{0}\rangle$, where $l \subset L$ is a subset of all links L including the empty set. Thus, the full local Hilbert space for our 2D model on a fixed triangulation $\mathcal{T}$ is

$$L^{2D}_{\mathcal{T}} = \bigoplus_{f\subset F}\bigoplus_{l\subset L}\left(\prod_{(ijk)\in f} c^\dagger_{(ijk)}|0\rangle \bigotimes \prod_{(ij)\in l} a^\dagger_{(ij)}|\tilde{0}\rangle \bigotimes \prod_{v\in V(\mathcal{T})} \mathbb{C}^{|G_b|}\right). \tag{1}$$

Here $|G_b|$ is the order of the bosonic symmetry group G_b. As a vector space, the fermionic Hilbert space on the triangles and links are the same as the tensor product $\bigotimes_{F(\mathcal{T})} \mathbb{C}^2 \otimes \bigotimes_{L(\mathcal{T})} \mathbb{C}^2$; however, the Fock space structure means that a local Hamiltonian for a fermion system is non-local when regarded as one for a boson system. We note that the above structure of total fermionic Hilbert space on arbitrary triangulations is slightly more general than Ref. 61, and it will allow us to construct very general FSET states in 2D. However, the constructions of general FSET states are beyond the scope of this paper.

As mentioned before, for FSPT states, the support space of FSLU transformations must be one dimensional since it can be connected to a product state in the absence of global symmetry. Therefore, the fermionic states of c and a fermions on the triangles and edges are completely fixed by the configurations of group elements $\{g_i\}$ on vertices. In particular, the complex fermion occupation number of c fermion is uniquely determined by the elements in $BH^2(G_b, \mathbb{Z}_2)$ (the obstruction free subgroup of $H^2(G_b, \mathbb{Z}_2)$), as first proposed by the special group super-cohomology construction of FSPT phases. Essentially, the complex fermion c can be regarded as a decoration on the intersection points of G_b-symmetry domain walls. In Ref. 50, 65, and 66, it was pointed out that a Majorana chain can be decorated onto the G_b-symmetry domain walls to generate a complete set of FSPT states in 2D. This layer of decoration is uniquely determined by the elements in $H^1(G_b, \mathbb{Z}_2)$. It requires a discrete spin structures and Kasteleyn orientations on the dual trivalent lattice (with a proper resolution for the lattice sites, as seen in Fig. 1), such that the total fermion parity of a fermion is always even on any closed loop, and we note that for FSPT state, the Majorana fermions must be paired up (see gray ellipse in Fig. 1) to form Kitaev's Majorana chains on the G_b symmetry domain walls (see green strip in Fig. 1). We will review all the details in section III A. An example of triangulation of torus and decoration of Kitaev's Majorana chains is given in Fig. 3. The full details will be discussed in section III B.

Thus, our 2D fixed-point state is a superposition of those basis states on all possible triangulations $\mathcal{T}$.

$$|\Psi\rangle = \sum_{\text{all conf.}} \Psi \left(\right) \Big| \left(\right) \Big\rangle. \tag{2}$$

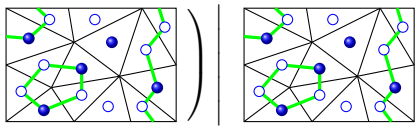

In section III B, we will derive the rules of wavefucntion renormalization generated by FSLU transformations. We will also obtain the conditions for fixed point wavefunction and show how to construct all FSPT states with total symmetry $G_f = G_b \times \mathbb{Z}_2^f$ on arbitrary triangulations in 2D. In the following, we would like to generalize all the above constructions into 3D.

The building block of bosonic and fermionic degrees of freedom is shown in Fig. 2. Again, every vertex i of the 3D space triangulation has a bosonic degree of freedom labelled by a group element $g_i \in G_b$. However, the spinless

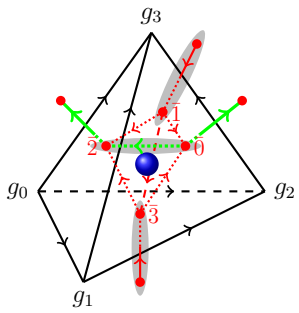

FIG. 2: Fermionic degrees of freedom in a tetrahedron. Red dots represent Majorana fermions at the two sides of each triangle. Blue ball represents the complex fermion of the (special) group super-cohomology model at the center of the tetrahedron. Green line is the decorated Kitaev's Majorana chain on the dual lattice $\mathcal{P}$.

complex fermion c introduced by group super-cohomology theory is now living on each tetrahedron (see blue ball in Fig. 2). In addition, each triangle of the space tetrahedron has two Majorana fermions on its two sides, which is again equivalent to a spinless complex fermion a. Similar to 2D case, let $|0\rangle$ and $|\tilde{0}\rangle$ be the ground states of no fermions on all tetrahedron and triangles, then a generating set of the Fock space is given by $\prod_{(ijkl)\in t} c^\dagger_{(ijkl)}|0\rangle \bigotimes \prod_{(ijk)\in f} a^\dagger_{(ijk)}|\tilde{0}\rangle$, where $t \subset T$ is a subset of all tetrahedra T including the empty set and $f \subset F$ is a subset of all triangles F including the empty set. Thus, the full local Hilbert space of our 3D model on a fixed triangulation $\mathcal{T}$ is:

$$L^{3D}_{\mathcal{T}} = \bigoplus_{t\subset T}\bigoplus_{f\subset F}\left(\prod_{(ijkl)\in t} c^\dagger_{(ijkl)}|0\rangle \bigotimes \prod_{(ijk)\in f} a^\dagger_{(ijk)}|\tilde{0}\rangle \bigotimes \prod_{v\in V(\mathcal{T})} \mathbb{C}^{|G_b|}\right). \tag{3}$$

Similar to the 2D case, the fermionic states of c and a fermions on the tetrahedra and triangles are also completely fixed by the configurations of group elements $\{g_i\}$ on vertices. The complex fermion occupation number of c fermion is uniquely determined by the elements in $BH^3(G_b, \mathbb{Z}_2)$ (the obstruction free subgroup of $H^3(G_b, \mathbb{Z}_2)$), which was also first proposed by the special group super-cohomology construction of FSPT states. It is not a surprise that in 3D the complex fermion c can also be regarded as a decoration (subjected to obstructions) on the intersection points of G_b-symmetry domain walls. The most interesting new feature here is that a Majorana chain can also be decorated onto the intersection lines of G_b-symmetry domain walls, and such a construction will generate a new set of FSPT states in 3D! As expected, this layer of decoration also requires a discrete spin structure on the dual trivalent lattice (with a proper resolution for the lattice sites as well, as seen in Fig. 2), and the Majorana fermions must be also be paired up to form Kitaev's Majorana chains (see green line in Fig. 2). However, such kind of decorations will be subjected to a fundamental obstruction on $H^4(G_b, \mathbb{Z}_2)$ due to fermion parity conservation. We will discuss all the details in section IV A. Furthermore, the fixed point condition of wavefunction renormalization will give rise to a secondary obstruction on $H^5(G_b, U_T(1))$. We will explore full details in section IV B.

Finally, our 3D fixed-point state is a superposition of those basis states on all possible triangulations $\mathcal{T}$:

$$|\Psi\rangle = \sum_{\text{all conf.}} \Psi \left(\right) \Big| \left(\right) \Big\rangle. \tag{4}$$

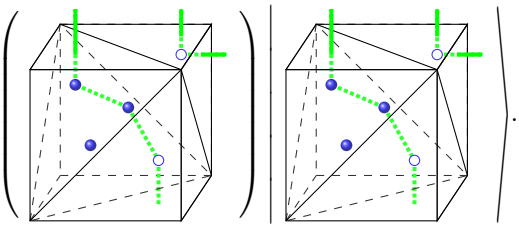

In section IV B, we will derive the rules of wavefucntion renormalization generated by FSLU transformations. We will also obtain the conditions for fixed point wavefunction and show how to construct all FSPT states with total symmetry $G_f = G_b \times \mathbb{Z}_2^f$ on arbitrary triangulations in 3D.

III. CONSTRUCTIONS AND CLASSIFICATIONS FOR FSPT STATES IN 2D

In Ref. 65, it was first pointed out that discrete spin structure and Kasteleyn orientations play an essential role for constructing FSPT phases with a decoration of Kitaev's Majorana chains on G_b-symmetry domain walls. In this

section, we will give a brief review of the essential idea and generalize the constructions onto arbitrary triangulations in 2D (see Fig. 3). In particular, we use Poincaré dual to show how to implement discrete spin structure and Kasteleyn orientations in 2D. The Poincaré dual will enable us to define discrete spin structure in arbitrary dimensions and give rise to the notion of *local* Kasteleyn orientations, which serves as the key step towards decorating Kitaev's Majorana chains onto the intersection lines of G_b-symmetry domain walls in higher dimensions.

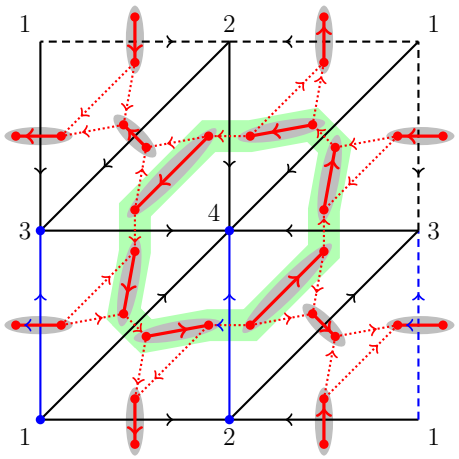

FIG. 3: Example of triangulation $\mathcal{T}$ of torus and Kitaev chain decoration. All vertices $\langle 1\rangle$, $\langle 2\rangle$, $\langle 3\rangle$ and $\langle 4\rangle$ (blue dots) are singular vertices, i.e., $w_0 = \langle 1\rangle + \langle 2\rangle + \langle 3\rangle + \langle 4\rangle$. We choose link $\langle 13\rangle$ and $\langle 24\rangle$ (blue lines) to be singular lines, i.e., $w_0 = \partial(\langle 13\rangle + \langle 24\rangle)$. The direction of the red links dual to $\langle 13\rangle$ and $\langle 24\rangle$ are changed. Vertices $i = 1, 2, 3, 4$ of $\mathcal{T}$ are labelled by group elements $g_i \in G$. Majorana fermions (red dots) live on vertices of the resolved dual lattice $\tilde{\mathcal{P}}$ (solid and dashed red links). Solid red links and gray ellipses indicate that the two Majorana fermions at its two ends are paired up, with respect to the link direction. Green strip is the $\mathbb{Z}_2$ domain wall of the "spin" configuration $\{g_i\}$ and is decorated by a Kitaev's Majorana chain (Majorana fermions along the domain wall are paired up differently from the "vacuum").

A. Discrete spin structure and Kasteleyn orientations

1. *Discrete Stiefel-Whitney homology class w_0*

It is well known that an oriented manifold M (with dimension n) admits spin structures if and only if its second Stiefel-Whitney class $[w^2] \in H^2(M, \mathbb{Z}_2)$ vanishes. In the construction of lattice models (on triangulation of M), we find it is more convenient to use the $(n-2)$-th Stiefel-Whitney homology class $[w_{n-2}]$ which is the Poincaré dual of $[w^2]$.

In this subsection, we only consider the 2D case. For a spatial manifold M ($n = 2$) with triangulation $\mathcal{T}$, the Stiefel-Whitney homology class $[w_0]$ has a representative which is the summation of all vertices v with some (mod 2) coefficients as follows [67] [68]:

$$w_0 = \sum_{v\in\mathcal{T}} \#\{\sigma | v \subseteq \sigma \text{ is regular}\} \cdot v. \tag{5}$$

Here, $v \subseteq \sigma$ means that v is a sub-simplex of simplex σ. $v \subseteq \sigma$ is called regular if v and σ have one of the three relative positions shown in Fig. 4. $\#\{\sigma | v \subseteq \sigma \text{ is regular}\} \cdot v$ denotes the formal product of the (mod 2) number of regular pairs $v \subseteq \sigma$ and the vertex v. We will call a vertex v singular if $\#\{\sigma | v \subseteq \sigma \text{ is regular}\}$ is odd. In this language, w_0 in Eq. (5) is the formal summation of all singular vertices. w_0 is a vector (0-th singular chain) in the vector space (of 0-th singular chains) spanned by formal bases of all vertices with $\mathbb{Z}_2$ coefficients.

It is known that all oriented 2D surfaces admit spin structures. In other words, the second Stiefel-Whitney class $[w^2]$, or the zeroth Stiefel-Whitney homology class $[w_0]$, of any oriented surface is (co)homologically trivial. As a result, the collection of singular vertices w_0 in Eq. (5) can be viewed as a boundary ∂S for some lines S (we will call them singular lines). For a fixed collection of singular vortices (a fixed representative w_0 for $[w_0]$), different inequivalent choices of singular lines S correspond to different spin structures which are isomorphic to $H^1(M, \mathbb{Z}_2)$ non-canonically. The singular lines S will be colored blue in the following figures.

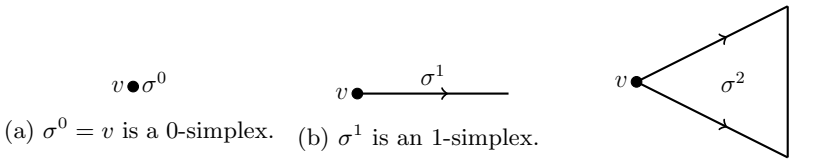

(a) $\sigma^0 = v$ is a 0-simplex. (b) σ^1 is an 1-simplex. (c) σ^2 is a 2-simplex.

FIG. 4: Regular pair $v \subseteq \sigma^i$ $(i = 0, 1, 2)$ for vertex v.

2. *Kasteleyn orientations and gauge transformations*

To decorate Kitaev chains to domain walls of a 2D spin model, it is useful to find out Kasteleyn orientations [62] for edges of the lattice [65, 66]. In this section, we will relate the existence of discrete spin structures (the vanishing of $[w_0]$) of a triangulation $\mathcal{T}$ to the existence of Kasteleyn orientations of the resolved dual lattice. Then in the next section, we can use FSLU transformations [28, 61] to classify FSPT states and define exactly solvable models on arbitrary triangulation lattices.

Our set up begins with a fixed triangulation $\mathcal{T}$ of the surface M. The first step is to construct a polyhedral decomposition $\mathcal{P}$ of M which is a trivalent graph dual to $\mathcal{T}$. We add a spinless fermionic degree of freedom to every link of $\mathcal{T}$ and split it into two Majorana fermions on the two sides of this link for convenience. Or equivalently, we can resolve the triangulation $\mathcal{T}$ by adding a new vertex to each triangle center and obtain a new triangulation $\tilde{\mathcal{T}}$. The Majorana fermions live on the vertices of the resolved dual lattice $\tilde{\mathcal{P}}$, which is a trivalent graph dual to $\tilde{\mathcal{T}}$ (see Fig. 5 and Fig. 3 for this construction on torus).

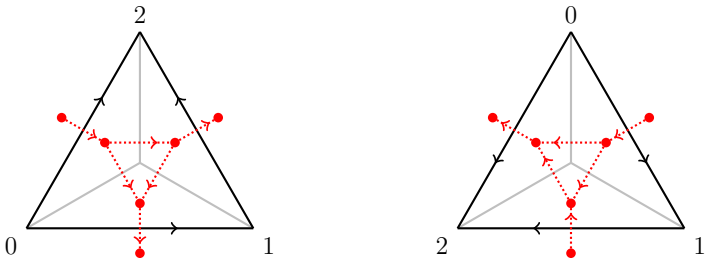

(a) Positive oriented triangle (b) Negative oriented triangle

FIG. 5: Triangulation $\mathcal{T}$ (black line), resolved triangulation $\tilde{\mathcal{T}}$ (black and gray line) and resolved dual lattice $\tilde{\mathcal{P}}$ (dashed red line). The resolved triangulation $\tilde{\mathcal{T}}$ is obtained from the original one $\mathcal{T}$ by adding a new vertex to the center of each triangle. The links of $\mathcal{P}$ have orientations induced from the link orientations of $\mathcal{T}$ according to the conventions shown in Fig. 6a. Red dots on vertices of $\tilde{\mathcal{P}}$ represent Majorana fermions which are split from complex fermions on each link of $\mathcal{T}$ (see discussions in section III B).

(a) Orientation convention for (red) link dual to (black) link $l \notin S$. (b) Orientation convention for (red) link dual to (blue) singular link $l \in S$.

FIG. 6: Conventions for orientations of links in $\tilde{\mathcal{P}}$ (dotted red line) from branching structure of triangulation $\mathcal{T}$ (solid black line). Non-singular (singular) black (blue) link $l \notin S$ ($l \in S$) induces orientation convention for the dual link in $\tilde{\mathcal{P}}$. We introduce a spinless fermion on each (black/blue) link in $\mathcal{T}$ and split it into two Majorana fermions on two sides of this link or vertices of $\tilde{\mathcal{P}}$ (red dots).

The second step is adding directions to links in $\mathcal{T}$ and $\tilde{\mathcal{P}}$. We order all the vertices in $\mathcal{T}$ and use the convention that all links are from vertices of smaller number to vertices of larger number. This is a branching structure of $\mathcal{T}$ such that there is no cycle for any triangle. The dual link direction in $\mathcal{P}$ is obtained from $\mathcal{T}$ using the convention shown

in Fig. 6a. The directions of new links in $\tilde{\mathcal{P}}$ are also obtained from the triangulation $\mathcal{T}$, by using the conventions in Fig. 5.

The essential point of the above link orientation conventions is as follows. When going along the smallest red loop in $\tilde{\mathcal{P}}$ around a vertex $v \in \mathcal{T}$ counterclockwise, we will encounter even number (due to the resolvation) of red links with the direction along or opposite to our direction (for example, the red loop inside the green strip around vertex 4 in Fig. 3). Using the conventions in Fig. 5, the red link direction is opposite to the counterclockwise direction if and only if: (1) The red link is dual to a black link in $\mathcal{T}$ such that v is the initial point of this black link. This corresponds to the case in Fig. 4b; (2) The red link is a resolved new link inside a triangle in $\mathcal{T}$ such that v is the first point of this triangle, i.e. the 0 point of the triangle $\langle 012\rangle$. This is the case in Fig. 4c. If the total number of the red links with opposite direction is odd, the vertex v will be called Kasteleyn-oriented. Since the smallest loop in $\tilde{\mathcal{P}}$ around v has even number of red links, it does not matter whether we use counterclockwise or clockwise conventions. Under the above construction, we relate the zeroth Stiefel-Whitney homology class w_0 in Eq. (5) and the orientations of links in $\tilde{\mathcal{P}}$, i.e. w_0 is the summation of all non-Kasteleyn-oriented vertices:

$$\begin{aligned} w_0 &= \sum_{v\in\mathcal{T}} \left(1 + \#\{\sigma^1 | v \subseteq \sigma^1 \text{ is regular}\} + \#\{\sigma^2 | v \subseteq \sigma^2 \text{ is regular}\}\right) \cdot v \\ &= \sum_{v\in\mathcal{T}} v \ (v \text{ is non-Kasteleyn-oriented}). \end{aligned} \tag{6}$$

Since the zeroth Stiefel-Whitney homology class $[w_0]$ for any oriented surface is trivial, we have $w_0 = \partial S$ for some singular line S. If we further reverse the directions of links in $\tilde{\mathcal{P}}$ crossing the singular lines S as shown in Fig. 6b, then all the vertices in $\mathcal{T}$ will be Kasteleyn-oriented. This is because this operation only changes the Kasteleyn property of the singular vertices in w_0 while preserving this property for all other vertices, including those in the interval of S. After all the above procedure, we relate the vanishing of the zeroth Stiefel-Whitney homology class $[w_0]$ to the property of Kasteleyn orientation of the smallest loop around each vertex.

Note that the above construction of link directions in $\tilde{\mathcal{P}}$ depends on the choices of singular lines S. On the one hand, the local shape of S is not important, as long as ∂S are fixed. In fact, if we change the shape of S locally, the changes of link directions in $\tilde{\mathcal{P}}$ can be obtained by several "gauge transformations" of Kasteleyn orientations, which relate two different but equivalent Kasteleyn orientations (simultaneously changing the directions of links sharing a common vertex in $\tilde{\mathcal{P}}$) [63]. An example of the basic shape changes of singular lines on $\mathcal{T}$ and gauge transformation of Kasteleyn orientations on $\tilde{\mathcal{P}}$ are shown in Fig. 7. Note that the Majorana degrees of freedom on vertices of $\tilde{\mathcal{P}}$ are mapped from one lattice to another according to the link directions under the gauge transformation of Kasteleyn orientations (n to n' in Fig. 7). In this way, the vacuum state without fermion (without Kitaev chain) on the left lattice is mapped to the vacuum state on the right lattice without fermion parity changing.

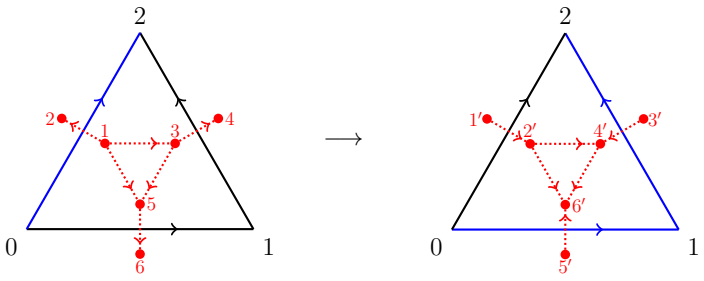

FIG. 7: Shape changing of singular lines S of $\mathcal{T}$ and "gauge transformation" of Kasteleyn orientations of $\tilde{\mathcal{P}}$. We perform "gauge transformations" on the three red vertices inside a black triangle, which effectively change the shape of S and the directions of three outreaching red links. The Majorana fermions are mapped from n to n' ($n = 1, 2, \cdots, 6$) with respect to the directions of red links dual to black links under this FSLU.

On the other hand, the homology class of S matters. Different choices of topological classes of S (fixed $w_0 = \partial S$) correspond to different spin structures on M. Our constructions make sure that, for arbitrary choices of S, the *local* Kasteleyn properties along the smallest loop around every vertex is satisfied. But the *global* Kasteleyn property along non-trivial cycles of M can be either preserved or broken. They correspond to 2^{2g} different spin structures on closed oriented surface M with genus g [63, 64]. Different choices of S induce different global Kasteleyn properties and thus correspond to different spin structures.

3. Kasteleyn orientations under retriangulations

In the above subsection, we only focus on a fixed triangulation $\mathcal{T}$ of M and relate its discrete Stiefel-Whitney homology class $[w_0]$ to the Kasteleyn orientations and spin structures. In order to use FSLU transformations to classify FSPT phases, we have to understand the relation of Kasteleyn orientations for different triangulations. In fact, we only have to find out the changes of Kasteleyn orientations under Pachner moves, which are basic moves of retriangulations [69].

Ordinary Pachner moves for two dimensional manifold consist of (2-2) move and (1-3) move. With branching structure, there are 3 types of (2-2) moves and 4 types of (1-3) moves in total (we do not consider the mirror images of these moves, otherwise the number of moves will be doubled). Only 2 types of (2-2) moves and 2 types of (1-3) moves have branching structure that can be induced by a global time ordering [42]. Examples of these moves are shown as follows:

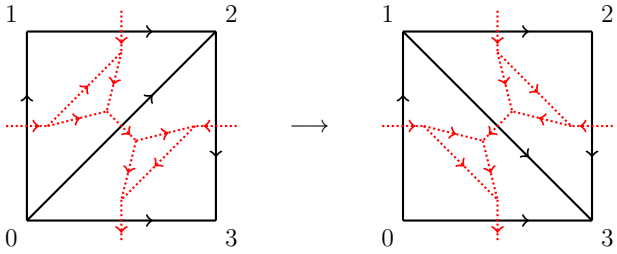

FIG. 8: Standard (2-2) move.

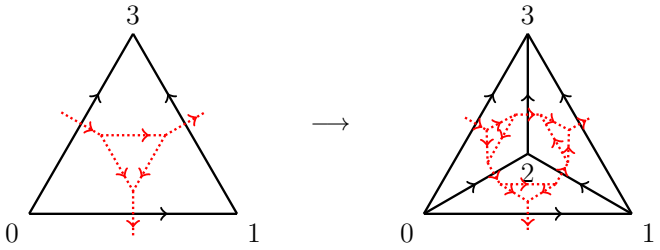

FIG. 9: One of (1-3) moves.

Other types of (2-2) and (1-3) moves are shown in Appendix A. For Pachner moves not induced by a global time ordering, the representative w_0 of Stiefel-Whitney class $[w_0]$ in Eq. (5) may be changed. For Pachner moves that are induced by a global time ordering, the representative w_0 of Stiefel-Whitney class $[w_0]$ is unchanged. This makes 2D case much easier than the 3D case.

B. Fermionic symmetric local unitary transformations and consistent equations

In the above section, we discussed discrete spin structure and Kasteleyn orientation construction on arbitrary 2D triangulation lattice. We can now decorate Kitaev's Majorana chains using these rules and systematically classify 2D FSPT states using FSLU transformations.

1. Decoration of Kitaev's Majorana chains

As discussed above, our model has two types of fermionic degrees of freedom. The first type is the complex fermion $c_{(ijk)}$ which lives at the center of triangle $\langle ijk\rangle$ of space manifold triangulation $\mathcal{T}$. We use $n_2(g_i, g_j, g_k) = 0, 1$ to denote the number of c fermion at the triangle $\langle ijk\rangle$. In fact, the parity conservation constraint for c fermions under retriangulation is $\mathrm{d}n_2 = 0 \pmod 2$. Therefore n_2 is an element of $H^2(G_b, \mathbb{Z}_2)$.

The second type of (complex) fermion $a_{(ij)}$ lives on the link $\langle ij\rangle$ of $\mathcal{T}$. In order to describe Kitaev's Majorana chain more conveniently, we separate the fermion $a_{(ij)}$ to two Majorana fermions:

$$\gamma_{ijA} = a_{(ij)} + a^\dagger_{(ij)}, \tag{7}$$

$$\gamma_{ijB} = \frac{1}{i}\left(a_{(ij)} - a^\dagger_{(ij)}\right). \tag{8}$$

The Majorana fermions γ_{ijA} and γ_{ijB} live on the two sides of link $\langle ij\rangle$. Dually, they live on the two ends of the link in $\tilde{\mathcal{P}}$ dual to link $\langle ij\rangle$. Our convention is that the dual link has direction from vertex $\langle ijA\rangle$ to $\langle ijB\rangle$. The fermion parity operator of a fermion or γ fermion at link $\langle ij\rangle$ is $P_f^\gamma = -i\gamma_{ijA}\gamma_{ijB}$.

Now let us decorate Kitaev's Majorana chains to the dual lattice. We use a $\mathbb{Z}_2$-valued 1-cochain $\tilde{n}_1(g_i, g_j)$ to indicate whether there is a domain wall between vertices i and j. $\tilde{n}_1 \in H^1(G_b, \mathbb{Z}_2)$ is a cocycle because we are constructing SPT states without deconfined Majorana fermions (the Kitaev chains should form closed loops). Depending on the configurations of $\{g_i\}$ and choices of $\tilde{n}_1$, the domain wall configuration in a particular lattice is different. We pair up the Majorana fermions depending on the domain wall configuration as follows: if there is no domain wall on link $\langle ij\rangle$, then the Majorana fermions γ_{ijA} and γ_{ijB} on the two sides of this link are paired up (vacuum pair) with respect to the direction of the dual red link (we use solid blue line and gray ellipse to indicate this pairing); if there is domain wall on link $\langle ij\rangle$, then the Majorana fermion of this link is paired up to another Majorana fermion, belonging to another links with domain wall, within the same triangle.

After fermion decoration, the (2-2) move becomes a fermionic unitary transformation between the fermionic Fock spaces on two different triangulation lattices $\mathcal{T}$ and $\mathcal{T}'$. An example of this standard F move is (there are $\mathbb{Z}_2$ domain walls on links $\langle 01\rangle$, $\langle 02\rangle$, $\langle 03\rangle$, and no domain wall on other links):

Ψ 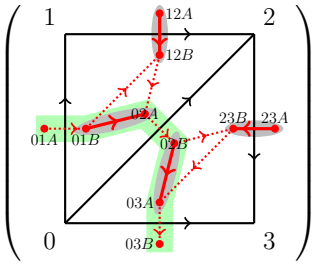 $= F(g_0,g_1,g_2,g_3)\ \Psi$ 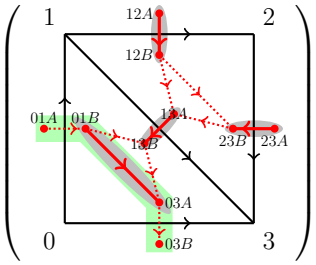 , (9)

where the F operator is defined as

$$F(g_0,g_1,g_2,g_3) = \nu_3(g_0,g_1,g_2,g_3) c^{\dagger n_2(g_0,g_1,g_2)}_{(012)} c^{\dagger n_2(g_0,g_2,g_3)}_{(023)} c^{n_2(g_0,g_1,g_3)}_{(013)} c^{n_2(g_1,g_2,g_3)}_{(123)} X[\tilde{n}_1(g_i,g_j)]. \tag{10}$$

Here, $\nu_3(g_0,g_1,g_2,g_3)$ is a $U_T(1)$-valued 3-cochain and $c^\dagger_{(012)}$ is the creation operator for c fermions at triangle $\langle 012\rangle$, etc. $X[\tilde{n}_1(g_i,g_j)]$ is a projection operator changing the Majorana fermion configurations. In the above example, X operator has an explicit form:

$$X[\tilde{n}_1] = 2^{1/2}\left(P_{01B,02A}P_{02B,03A}\right)P_{13A,13B}, \tag{11}$$

where $P_{a,b} = (1 - i\gamma_a\gamma_b)/2$ is the projection operator for Majorana pairs $\langle a, b\rangle$ (the direction is from vertex a to vertex b). The first two projection operators in the above equation project the state to the Majorana dimer configuration in the left figure. Note that the Majorana fermions which do not appear explicitly on one lattice are considered to be in the vacuum pairs. For example, the two Majorana fermions γ_{13A} and γ_{13B} only appear in the right figure. They are considered to be paired from γ_{13A} to γ_{13B} in the left figure. Therefore, we have a third projection operator in Eq. (11) to put the two Majorana fermions γ_{13A} and γ_{13B} to vacuum state ($a^\dagger_{(13)}a_{(13)} = 0$) in the left figure. All other Majorana fermions that are not shown in Eq. (11) are unchanged under the above F move.

Since we are constructing FSPT states, the fermionic local unitary transformation F should be G_b symmetric in the sense that

$$F(g_0,g_1,g_2,g_3) = F(gg_0, gg_1, gg_2, gg_3), \tag{12}$$

for all $g \in G_b$ if G_b is a unitary symmetry group. That is why $\nu_3(g_0,g_1,g_2,g_3)$, $n_2(g_0,g_1,g_2)$ and $\tilde{n}_1(g_0,g_1)$ are all cochains which are invariant under unitary g action.(We note that $\nu_3(gg_0,gg_1,gg_2,gg_3) = \nu_3^*(g_0,g_1,g_2,g_3)$ for antiunitary g action.)

In general, there are eight kinds of domain wall configurations in the above F move. One can show that for all configurations, the fermion parities of Majorana fermions are the same in the initial and final wave functions (this comes from the Kasteleyn orientation property of retriangulations, see section III A and Appendix A). Therefore, the fermion parities of c fermions and γ fermions should also be conserved separately, and both $n_2 \in H^2(G_b, \mathbb{Z}_2)$ and $\tilde{n}_1 \in H^1(G_b, \mathbb{Z}_2)$ are cocycles.

The phase factor in the front of the F operator can be changed from ν_3 to

$$\nu_3'(g_0,g_1,g_2,g_3) = \nu_3(g_0,g_1,g_2,g_3)\frac{\mu_2(g_1,g_2,g_3)\mu_2(g_0,g_1,g_3)}{\mu_2(g_0,g_2,g_3)\mu_2(g_0,g_1,g_2)}, \tag{13}$$

where $\mu_2(g_0,g_1,g_2)$ is a $U_T(1)$-valued 2-cochain. If $\nu_3(g_0,g_1,g_2,g_3)$ is a consistent solution of fixed-point state (see section III B 2), so is $\nu_3'(g_0,g_1,g_2,g_3)$. However, we can use a FSLU transformation U_{μ_2,m_1} to smoothly connect the these two fixed-point states with ν_3 and ν_3' in F symbols. The FSLU transformation U_{μ_2,m_1} decorates fermions to the links of the triangulation and is defined as

$$U_{\mu_2,m_1}|\{g_l\}\rangle = \prod_{\langle ijk\rangle} \mu_2(g_i,g_j,g_k)^{s_{\langle ijk\rangle}} \prod_{\langle ij\rangle} f_{(ij)}^{\dagger m_1(g_i,g_j)}|\{g_l\}\rangle, \tag{14}$$

where $s_{\langle ijk\rangle} = \pm 1$ is the orientation of the triangle $\langle ijk\rangle$, and $f_{(ij)}$ is the annihilation operator of the new fermions decorated on the link $\langle ij\rangle$. Although we decorate new f fermions with fermion number m_1 to the links, it does not induce additional sign factor[42]. So the equivalence relation of ν_3' and ν_3 in Eq. (13) is the same as the bosonic one. Therefore, elements ν_3 in the group cohomology class $H^3(G_b, U_T(1))$ correspond to the same 2D FSPT phase [42].

Apart from the (2-2) move, there is another (2-0) move which plays the role of unitary condition. An example of domain wall configurations for (2-0) move is

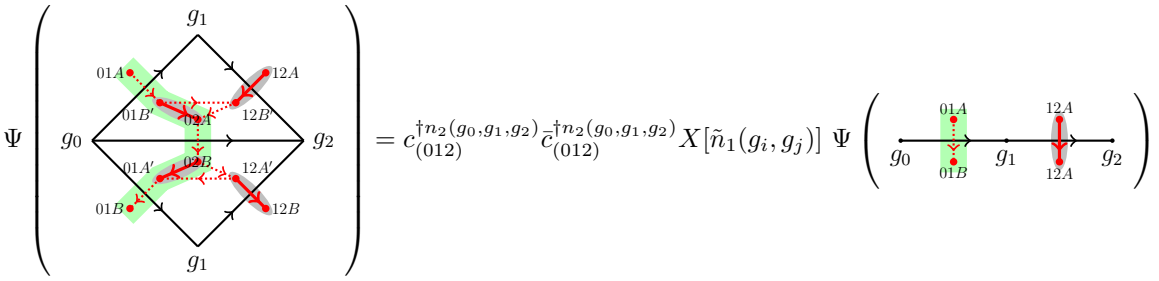

where $c_{(012)}$ and $\bar{c}_{(012)}$ are the annihilation operators of the c fermions at the center of two triangles with opposite orientation in the left figure. $X[\tilde{n}_1]$ is also the projection operator from the state of Majorana dimer pairs in the right figure to the state of the left figure. Note that there are six Majorana fermions $(\gamma_{02A}, \gamma_{02B}, \gamma_{01A'}, \gamma_{01B'}, \gamma_{12A'}, \gamma_{12B'})$ that do not appear explicitly in the right figure. Similar to the case of (2-2) move, they should also be considered to be in vacuum pairs in the right figure state, such that $-i\gamma_{02A}\gamma_{02B} = -i\gamma_{01B'}\gamma_{01A} = -i\gamma_{12B'}\gamma_{12A'} = 1$ when acting on the right figure state. This choice is possible because the dimer loop $01A$-$01B'$-$01A'$-$01B$-$01A$ is Kasteleyn oriented. Therefore one can also use the convention that the two Majorana fermions on the two sides of a link are paired up, by regarding the projection operators $-i\gamma_{01A}\gamma_{01B'}, -i\gamma_{01A'}\gamma_{01B}, -i\gamma_{12A}\gamma_{12B'}, -i\gamma_{12A'}\gamma_{12B}$ as 1 when acting on the vacuum state of the left figure. The X operator then projects the state to the Majorana dimer configuration state in the left figure. The fermion parities of the left and right states are always the same. An explicit expression of X for this particular (2-0) move is

$$X[\tilde{n}_1] = 2P_{01B',02A}P_{02B,01A'}P_{12A,12B'}P_{12A',12B}. \tag{16}$$

Using the (2-0) moves, we can deduce all (3-1) moves and other (2-2) moves form the standard (2-2) F move in Eq. (9).

2. *Fermionic pentagon equations*

In the above section, we have discussed the FSLU moves. The most important one is the standard F move in Eq. (9). Similar to the bosonic pentagon equation for the bosonic F move, we have a fermionic pentagon equation as consistent equation for FSLU transformations (see Fig. 10). This fermionic pentagon equation only involves the standard F move. Using the unitary conditions, one can also derive other pentagon equations and they essentially give the same constraint for ν_3.

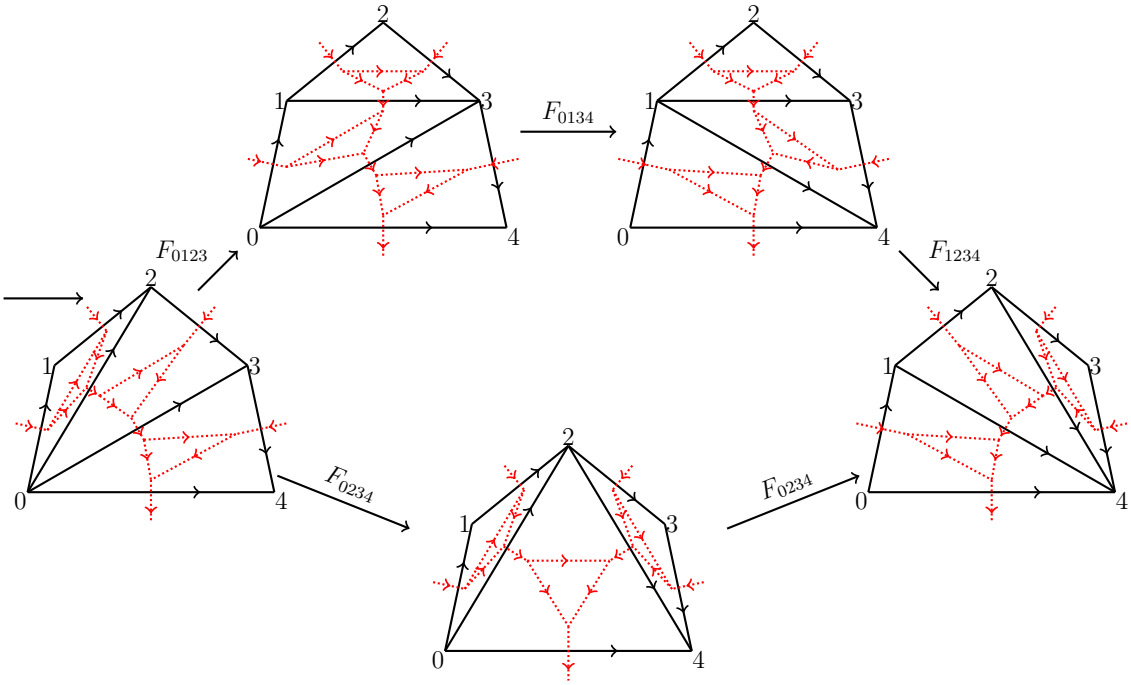

FIG. 10: Fermionic pentagon equation.

Let us now calculate the constraint for ν_3 from the pentagon equation in Fig. 10. Since the c fermions and Majorana fermions are decoupled (the c fermion part and Majorana fermion part of X in Eq. (10) commute) in the F move, only the c fermion will twist the cocycle condition for ν_3. The X operators are merely projection operators that do not introduce any nontrivial phases in two different paths of pentagon equation. The final result of equation for ν_3 is the same as the (special) group super-cohomology theory [42, 61], i.e.,

$$(\mathrm{d}\nu_3)(g_0,g_1,g_2,g_3,g_4) = (-1)^{Sq^2(n_2)(g_0,g_1,g_2,g_3,g_4)} = (-1)^{n_2(g_0,g_1,g_2)n_2(g_2,g_3,g_4)}. \tag{17}$$

Now, we see that only $BH^2(G_b,\mathbb{Z}_2)$, the obstruction free subgroup of $H^2(G_b,\mathbb{Z}_2)$ formed by elements $n_2 \in H^2(G_b,\mathbb{Z}_2)$ that satisfy $Sq^2(n_2)=0$ in $H^4(G_b,U_T(1))$ can give rise to solutions for ν_3, and inequivalent solutions of ν_3 is still given by $H^3(G_b,U_T(1))$ according to the gauge transformations of ν_3. In conclusion, the mathematical objects that classify 2D FSPT phases with a total symmetry $G_f = G_b \times \mathbb{Z}_2^f$ can be summarized as three group cohomologies of the symmetry group [48, 50]: $H^1(G_b,\mathbb{Z}_2)$, $BH^2(G_b,\mathbb{Z}_2)$ and $H^3(G_b,U_T(1))$. Finally, by using the method proposed in Ref. 61, one can derive the commuting projector parent Hamiltonian of all these FSPT states on arbitrary 2D triangulations(with a branching structure).

IV. CONSTRUCTIONS AND CLASSIFICATIONS FOR FSPT STATES IN 3D

In this section, we will classify the 3D FSPT states parallel to the discussions of 2D FSPT states. Compared to the 2D case, the most nontrivial part of 3D phases are the fermion parity mixing of the c fermions and Majorana fermions. In section IV A, we find that there are in general no Kasteleyn orientations on a 3D lattice. The existence of spin structure only implies *local* Kasteleyn orientations. If we decorate Kitaev's Majorana chains to 3D lattice, the shape changing process of the chain may change the fermion parity of the Majorana fermions. In this case, we should use the c fermion to compensate the fermion parity changes. Because of the fermion parity mixing, the cocycle equation for ν_4 is much more complicated than the special group super-cohomology model.

A. Discrete spin structure in 3D and local Kasteleyn orientations

In this subsection, we will discuss the first Stiefel-Whitney homology class on discrete lattice and relate it to the *local Kasteleyn orientations* on the dual lattice. The overall constructions are parallel to the 2D case. The difference

is that Kasteleyn orientations are only satisfied for the smallest loops in 3D, not for the general large loops. The fermion parity of Kitaev chain decorated on fluctuating loop is therefore not conserved.

1. *Discrete Stiefel-Whitney homology class w_1*

Similar to the oriented 2D manifolds, all oriented 3D manifolds admit spin structures. The second Stiefel-Whitney cohomology class $[w^2]$ is always trivial. Dually, we can consider the first discrete Stiefel-Whitney homology class for a triangulation $\mathcal{T}$ (with branching structure) of 3D spatial manifold M [67]:

$$w_1 = \sum_{l\in\mathcal{T}} \#\{\sigma | l \subseteq \sigma \text{ is regular}\} \cdot l. \tag{18}$$

w_1 is the summation of all links in $\mathcal{T}$ with some $\mathbb{Z}_2$ coefficients. Again, $l \subseteq \sigma$ means that link l is a sub-simplex of simplex σ. And $l \subseteq \sigma$ is called regular if l and σ have one of the three relative positions shown in Fig. 11. If $\#\{\sigma | l \subseteq \sigma \text{ is regular}\}$ is odd, we will call the link l singular. So w_1 in Eq. (18) is the formal summation of all singular lines. w_1 is a vector (1-th singular chain) in the vector space (of 1-th singular chains) spanned by formal bases of all links with $\mathbb{Z}_2$ coefficients.

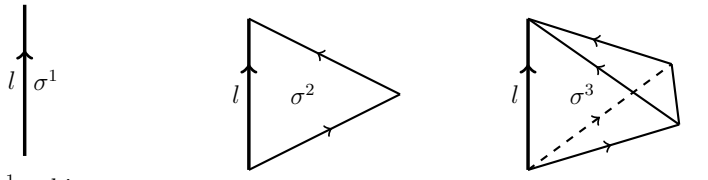

(a) $\sigma^1 = l$ is an 1-simplex. (b) σ^2 is a 2-simplex. (c) σ^3 is a 3-simplex.

FIG. 11: Regular pairs $l \subseteq \sigma^i$ $(i = 1, 2, 3)$ for link l.

Since the second Stiefel-Whitney cohomology class $[w^2]$ of any oriented 3D manifold is trivial, we can find some surface S such that $w_1 = \partial S$. For a fixed collection of singular links (a fixed representative w_1 for $[w_1]$), different inequivalent choices of S correspond to different spin structures.

2. *Local Kasteleyn orientations and gauge transformations*

In 3D model, we also want to decorate Kitaev chains to some loops. A natural question inherited from 2D is whether there are Kasteleyn properties for all even-link loops in 3D. This is related to the fermion parity of the Kitaev chain. The answer is that the existence of discrete spin structures (the vanishing of $[w_1]$) is related to the existence of *local* Kasteleyn orientations of the resolved dual lattice. In other words, Kasteleyn properties are satisfied for the smallest loops, but broken for large loops in 3D in general.

Here is the construction which is similar to the 2D case. For a fixed triangulation $\mathcal{T}$ of 3D manifold M, the first step is to construct a polyhedral decomposition $\mathcal{P}$ of M which is a 4-valent graph dual to $\mathcal{T}$. We now add a spinless fermionic degree of freedom to every face (triangle) of $\mathcal{T}$ and split it into two Majorana fermions on the two sides of this face for convenience. Equivalently, we resolve the triangulation $\mathcal{T}$ by adding a new vertex to each tetrahedron center and obtain a new resolved triangulation $\tilde{\mathcal{T}}$. The Majorana fermions live on the vertices of the resolved dual lattice $\tilde{\mathcal{P}}$, which is a 4-valent graph dual to $\tilde{\mathcal{T}}$ (see Fig. 12).

The second step is again adding directions to links in $\mathcal{T}$ and $\tilde{\mathcal{P}}$. The directions of links in $\mathcal{T}$ are given by the branching structure. The dual link direction in $\mathcal{P}$ is obtained from $\mathcal{T}$ using the convention shown in Fig. 13a. The directions of new links in $\tilde{\mathcal{P}}$ are obtained from the triangulation $\mathcal{T}$, by using the conventions in Fig. 12.

The above link direction construction has the following properties. Consider a fixed link $l \in \mathcal{T}$. When going along the smallest red loop in $\tilde{\mathcal{P}}$ around this link l along the right-hand rule direction, we will encounter even number of red links with the direction along or opposite to our direction. Using the conventions in Fig. 12, the red link direction is opposite to our direction if and only if: (1) The red link is dual to a black triangle in $\mathcal{T}$ such that the initial and final vertices of l are the first and the last vertices of this black triangle. This corresponds to the case in Fig. 11b; (2) The red link is a resolved new link inside a tetrahedron in $\mathcal{T}$ such that the initial and final vertices of l are the first and the last vertices of this tetrahedron. This is the case in Fig. 11c. If the total number of the red links with opposite

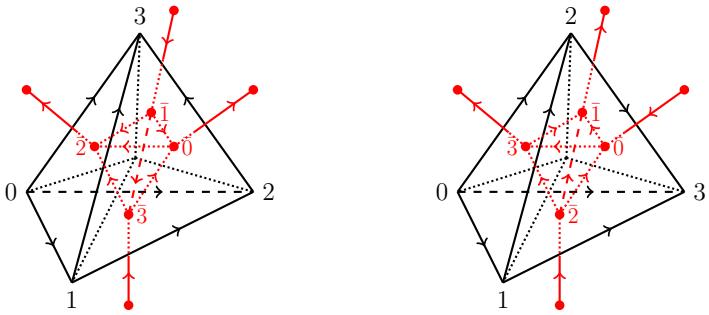

(a) Positive oriented tetrahedron (b) Negative oriented tetrahedron

FIG. 12: Triangulation $\mathcal{T}$ (solid black line), resolved triangulation $\tilde{\mathcal{T}}$ (solid and dashed black line) and resolved dual lattice $\tilde{\mathcal{P}}$ (red line). The resolved triangulation $\tilde{\mathcal{T}}$ is obtained from the original one $\mathcal{T}$ by adding a new vertex to the center of each tetrahedron. The links of $\mathcal{P}$ have orientations induced from the link orientations of $\mathcal{T}$ according to the conventions shown in Fig. 13a. Red dots on vertices of $\tilde{\mathcal{P}}$ represent Majorana fermions which are split from complex fermions on each face of $\mathcal{T}$.

(a) Orientation convention for (red) link dual to (black) triangle $f \notin S$.

(b) Orientation convention for (red) link dual to (blue) singular triangle $f \in S$.

FIG. 13: Conventions for orientations of links in $\tilde{\mathcal{P}}$ (red line) from branching structure of triangulation $\mathcal{T}$ (black line). Non-singular (singular) black (blue) triangle $f \notin S$ ($f \in S$) induces orientation for the dual link in $\tilde{\mathcal{P}}$. We introduce a spinless fermion on each (black/blue) triangle in $\mathcal{T}$ and split it into two Majorana fermions on two sides of this triangle or vertices of $\tilde{\mathcal{P}}$ (red dots).

direction is odd, we will call the link l Kasteleyn-oriented. Under this construction, we relate the first Stiefel-Whitney homology class w_1 in Eq. (18) to the orientations of links in $\tilde{\mathcal{P}}$, i.e. w_1 is the summation of all non-Kasteleyn-oriented links:

$$\begin{aligned} w_1 &= \sum_{l\in\mathcal{T}} \left(1 + \#\{\sigma^2 | l \subseteq \sigma^2 \text{ is regular}\} + \#\{\sigma^3 | l \subseteq \sigma^3 \text{ is regular}\}\right) \cdot l \\ &= \sum_{l\in\mathcal{T}} l \ (l \text{ is non-Kasteleyn-oriented}). \end{aligned} \tag{19}$$

As discussed above, the first Stiefel-Whitney homology class $[w_1]$ for any oriented 3D manifold is trivial. Therefore we have some singular surface S such that $w_1 = \partial S$. Now if we reverse the directions of links in $\tilde{\mathcal{P}}$ crossing the singular surface S as shown in Fig. 13b, then all the links in $\mathcal{T}$ will be Kasteleyn-oriented. After all the above procedures, we relate the vanishing of the zeroth Stiefel-Whitney homology class $[w_0]$ to the property of *local* Kasteleyn orientations of the smallest loops around all link in $\mathcal{T}$. Here, "local" means that only the smallest loops in $\tilde{\mathcal{P}}$ around links in $\mathcal{T}$ are Kasteleyn-oriented. Larger loops with even number of links do not have Kasteleyn property in general.

The above construction of link directions in $\tilde{\mathcal{P}}$ depends on the choices of singular surface S. The shape of S can be also changed with fixed ∂S. If we change the shape of S locally, the changes of link directions in $\tilde{\mathcal{P}}$ can be obtained by several "gauge transformations" of Kasteleyn orientations. We define this by simultaneously changing the directions of links sharing a common vertex in $\tilde{\mathcal{P}}$, similar to the 2D case [63]. Different Kasteleyn orientations related by this "gauge transformations" are said to be equivalent. An example of shape changes of singular surfaces on $\mathcal{T}$ and gauge transformation of Kasteleyn orientations on $\tilde{\mathcal{P}}$ are shown in Fig. 14. The Majorana degrees of freedom on vertices of $\tilde{\mathcal{P}}$ are also mapped from one lattice to another according to the link directions (similar to the 2D case in Fig. 7). This makes sure that the vacuum state (without Kitaev chain) on one lattice is mapped to the vacuum state on another lattice, without fermion parity changing (no fermion on both lattice).

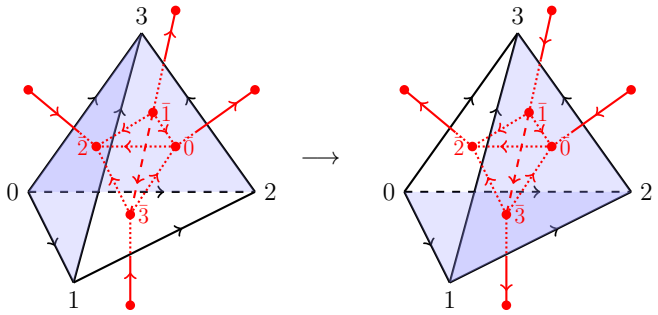

FIG. 14: Shape changing of singular surfaces S of $\mathcal{T}$ and "gauge transformation" of Kasteleyn orientations of $\tilde{\mathcal{P}}$. We perform "gauge transformations" on the four red vertices inside a black tetrahedron, which effectively change the shape of S and the directions of four outreaching red links. The Majorana fermions are mapped with respect to the directions of red links dual to black triangles under this FSLU transformation.

With fixed $w_0 = \partial S$, the choices of S are not unique. Different choices of topological classes of S correspond to different spin structures on M. This is because the global Kasteleyn properties along non-trivial cycles of M can also be either preserved or broken, depending on the choices of S. Our construction generalizes the relation of Kasteleyn orientations and spin structures in 2D [63] to 3D.

3. *Local Kasteleyn orientations under retriangulations*

In order to perform FSLU transformations, we now consider that the Kasteleyn orientation changes under retriangulations of M. Pachner moves for 3D manifold consist of (2-3) move and (1-4) move [69]. When introducing branching structure, there are totally 10 types of (2-3) moves and 5 types of (1-4) moves (again we do not consider the mirror images of these moves, otherwise the number will be doubled) [42]. 8 types of (2-3) moves and 3 types of (1-4) moves have branching structure that can be induced by global time ordering [42, 70]. The standard (2-3) move is given in Fig. 15, which do not involve singular surfaces. Two examples of the moves involving singular surfaces (the representative w_1 of Stiefel-Whitney class $[w_1]$ in Eq. (18) is changed) are presented in Figs. 16 and 17. Other types of (2-3) and (1-4) moves are shown in Appendix B.

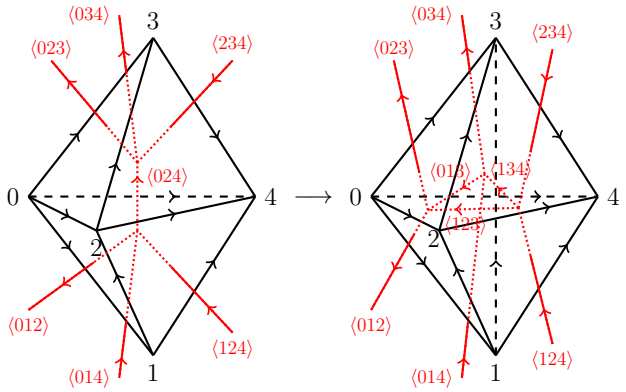

(a) For triangulation $\mathcal{T}$ and dual lattice $\mathcal{P}$.

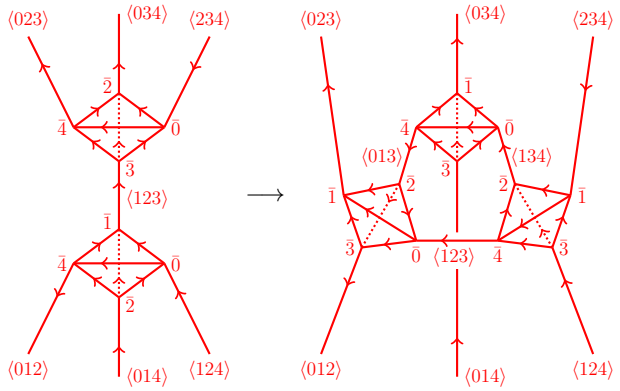

(b) For resolved dual lattice $\tilde{\mathcal{P}}$.

FIG. 15: Standard (2-3) move.

Until now, the construction in 3D is very similar to the 2D case. However, there is a very crucial difference. Although both the lattices before and after the Pachner move have *local* Kasteleyn properties, the Kasteleyn orientation for larger loops may be broken. Consider for example the case in Fig. 16. If we consider that the large loop consists of links $\langle 012\rangle$, $\langle 123\rangle$ and $\langle 124\rangle$ (and the new resolved links between them) on the left lattice $\tilde{\mathcal{P}}$, and links $\langle 012\rangle$ and $\langle 124\rangle$ (and the new resolved links between them) on the right lattice $\tilde{\mathcal{P}}'$, the Kasteleyn properties are the same (all 5 links on $\tilde{\mathcal{P}}$ and 3 links on $\tilde{\mathcal{P}}'$ have up direction). On the other hand, if we consider that the large loop consists of links

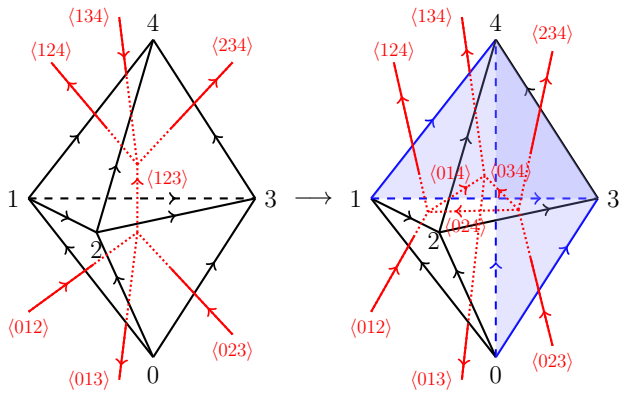

(a) (2-3) move for triangulation $\mathcal{T}$ and dual lattice $\mathcal{P}$. Singular links $w_1 = \langle 14\rangle + \langle 34\rangle + \langle 03\rangle + \langle 04\rangle$ and surfaces $S = \langle 034\rangle + \langle 134\rangle$ are represented by blue lines and blue triangles.

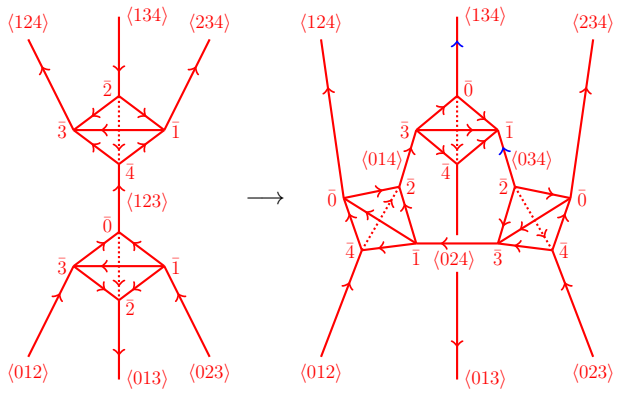

(b) (2-3) move for resolved dual lattice $\tilde{\mathcal{P}}$. Blue arrows on dual (red) links $\langle 034\rangle$ and $\langle 134\rangle$ indicate that the directions are reversed by singular surfaces S.

FIG. 16: One of (2-3) moves that involve singular surfaces.

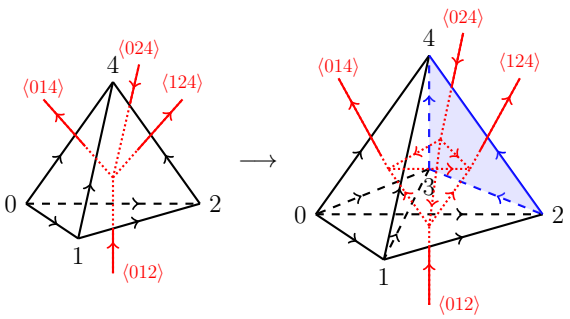

(a) (1-4) move for triangulation $\mathcal{T}$ and dual lattice $\mathcal{P}$. Singular links $w_1 = \langle 23\rangle + \langle 34\rangle + \langle 24\rangle$ and surfaces $S = \langle 234\rangle$ are represented by blue lines and blue triangles.

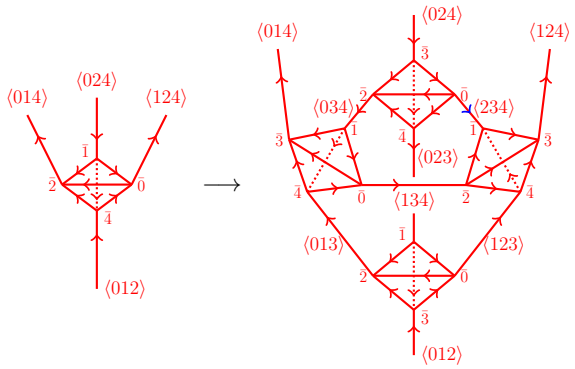

(b) (1-4) move for resolved dual lattice $\tilde{\mathcal{P}}$. Blue arrow on dual (red) links $\langle 234\rangle$ indicates that the directions are reversed by singular surfaces S.

FIG. 17: One of (1-4) moves.

$\langle 012\rangle$, $\langle 123\rangle$ and $\langle 234\rangle$ on the left lattice $\tilde{\mathcal{P}}$, and links $\langle 012\rangle$, $\langle 024\rangle$ and $\langle 234\rangle$ on the right lattice $\tilde{\mathcal{P}}'$, the Kasteleyn properties are changed (all 5 links on $\tilde{\mathcal{P}}$ have up direction, but only 2 of 5 links on $\tilde{\mathcal{P}}'$ have up direction). In next subsection, we will systematically analyze the Kasteleyn properties of loops under Pachner moves. After decorating Majorana fermions, we will known the Majorana fermion parity changes which are very important in constructing legitimate fermionic states.

B. Fermionic symmetric local unitary transformations and consistent equations

With the above setup of discrete spin structure and Kasteleyn orientation construction on 3D lattice, we can now use the FSLU transformation to classify 3D FSPT states systematically.

1. *Fermion parity and the obstruction of Kitaev's Majorana chain decoration*

Similar to the 2D case, our 3D model has two types of fermionic degrees of freedom. The first type is the complex fermion $c_{(ijkl)}$ which lives at the center of tetrahedron $\langle ijkl\rangle$ of triangulation $\mathcal{T}$ of space manifold. In the (special) group super-cohomology wave function, the c fermion parity P_f^c is unchanged under (2-3) and (1-4) moves. If we

use $n_3(g_i, g_j, g_k, g_l) = 0, 1$ to denote the number of c fermion at the tetrahedron $\langle ijkl\rangle$, then the parity conserved condition becomes $\mathrm{d}n_3 = 0 \pmod 2$. Therefore n_3 is an element of $H^3(G_b, \mathbb{Z}_2)$. This will be not true if we introduce the second type of fermions.

The second type of (complex) fermion $a_{(ijk)}$ lives on the triangle $\langle ijk\rangle$ of $\mathcal{T}$. Similar to the 2D case, we also separate the fermion $a_{(ijk)}$ to two Majorana fermions:

$$\gamma_{ijkA} = a_{(ijk)} + a^\dagger_{(ijk)}, \tag{20}$$

$$\gamma_{ijkB} = \frac{1}{i}\left(a_{(ijk)} - a^\dagger_{(ijk)}\right). \tag{21}$$

The Majorana fermions γ_{ijkA} and γ_{ijkB} live on the two sides of triangle $\langle ijk\rangle$, or dually, on two ends of the link in $\tilde{\mathcal{P}}$ dual to triangle $\langle ijk\rangle$. Our convention is that the dual link (we will also use $\langle ijk\rangle$ to denote the dual link) has direction from vertex $\langle ijkA\rangle$ to $\langle ijkB\rangle$. So the fermion parity operator of a fermion or γ fermion at triangle $\langle ijk\rangle$ is $P_f^\gamma = -i\gamma_{ijkA}\gamma_{ijkB}$.

Now let us decorate Kitaev's Majorana chains to the loops in dual lattice $\mathcal{P}$. We introduce a $\mathbb{Z}_2$ cochain $\tilde{n}_2(g_i, g_j, g_k) = 0, 1$ to specify the decoration configuration of Kitaev's Majorana chain. If there is a Kitaev chain goes though link $\langle ijk\rangle$ in $\mathcal{P}$ [see the green links in Fig. 2 and figures in Eq. (25)], then we set $\tilde{n}_2(g_i, g_j, g_k) = 1$. On the other hand, $\tilde{n}_2(g_i, g_j, g_k) = 0$ means there is no Kitaev chain. The Kitaev chain decorations can be translated to dimer configurations of Majorana pairs in the resolved dual lattice $\tilde{\mathcal{P}}$. $\tilde{n}_2(g_i, g_j, g_k) = 0$ indicates the vacuum pairing, i.e., the two Majorana fermions at triangle $\langle ijk\rangle$ are paired up from $\langle ijkA\rangle$ to $\langle ijkB\rangle$. If $\tilde{n}_2(g_i, g_j, g_k) = 1$, then γ_{ijkA} and γ_{ijkB} are paired up with other nearby Majorana fermions separately, similar to the construction of Kitaev's Majorana chain (see figures of Eq. (26) where gray ellipses indicate paired Majorana fermions).

Since we are constructing an SPT state without intrinsic anyonic excitations, the decorated Kitaev chain should form a closed loop without ends. Therefore, similar to the 2D case, we have the equation $\mathrm{d}\tilde{n}_2 = 0 \pmod 2$, which means that the cochain $\tilde{n}_2$ is an element of $H^2(G_b, \mathbb{Z}_2)$. It is possible that all the four faces of a tetrahedron $\langle 0123\rangle$ in $\mathcal{T}$ are decorated with Kitaev chains, i.e., $\mathrm{d}\tilde{n}_2(g_0, g_1, g_2, g_3) = 4$. There are ambiguities of pairing four Majorana fermions inside the tetrahedron. In the total three possible pairings , we use the convention that the Majorana fermion $\bar{0}$ is paired to $\bar{2}$, and $\bar{1}$ is paired to $\bar{3}$ (see Fig. 18). One can also choose other conventions which will essentially produce the same results [71].

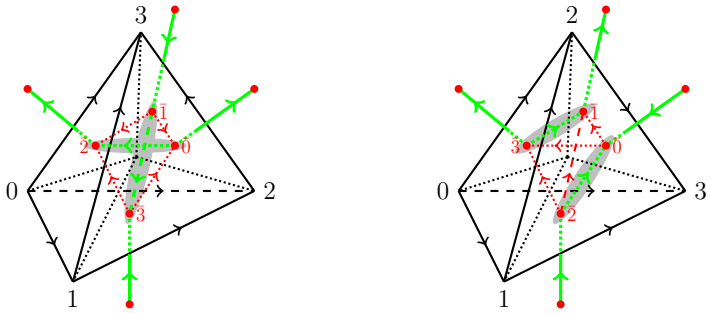

(a) Positive oriented tetrahedron (b) Negative oriented tetrahedron

FIG. 18: Resolvation of four strings of Kitaev's Majorana chains meeting at one tetrahedron. If four strings meet at one tetrahedron, we should pair the Majorana fermions $\bar{0}$ to $\bar{2}$ and $\bar{1}$ to $\bar{3}$, respectively (gray ellipses). The Green lines on $\tilde{\mathcal{P}}$ indicate that these lines are decorated by Kitaev chains.

Now let us turn to the Pachner moves for different triangulations. We find that the Majorana fermion parity is changed under (2-3) move if and only if

$$Sq^2(\tilde{n}_2)(g_0, g_1, g_2, g_3, g_4) = \tilde{n}_2(g_0, g_1, g_2)\tilde{n}_2(g_2, g_3, g_4) = 1. \tag{22}$$

We will use the notation $Sq^2(\tilde{n}_2) = \tilde{n}_2^2 = \tilde{n}_2 \smile \tilde{n}_2$ later. This can be obtained by directly checking the property of Kasteleyn orientation for loops in the transition graph of two Majorana dimer states for 64 kinds of string configurations of each (2-3) move (see Appendix B). To compensate the Majorana fermion parity changes, the fermion parity of the fermions at the center of tetrahedron should also be changed, leading to the (mod 2) equation

$$\mathrm{d}n_3 = \tilde{n}_2 \smile \tilde{n}_2, \tag{23}$$

or more explicitly:

$$n_3(g_1,g_2,g_3,g_4)+n_3(g_0,g_2,g_3,g_4)+n_3(g_0,g_1,g_3,g_4)+n_3(g_0,g_1,g_2,g_4)+n_3(g_0,g_1,g_2,g_3)=\tilde{n}_2(g_0,g_1,g_2)\tilde{n}_2(g_2,g_3,g_4). \tag{24}$$

The above equation shows that the cocycle equation of n_3 is twisted by $\tilde{n}_2^2$, which is different from $\mathrm{d}n_3=0$ in the (special) group super-cohomology model [42]. The above equation for n_3 has solutions if and only if $Sq^2(\tilde{n}_2)$ is the trivial element in $H^4(G_b,\mathbb{Z}_2)$.

2. *Fermionic symmetric local unitary transformations*

After fermion decoration, the standard (2-3) move Fig. 15 becomes a fermionic unitary transformation between the fermionic Fock spaces on two different triangulation lattices $\mathcal{T}$ (left) and $\mathcal{T}'$ (right). An example of this standard F move which changes the fermion parity of Majorana fermions is (on lattice $\mathcal{T}$, $\mathcal{P}$ in Eq. (25) and on $\tilde{\mathcal{P}}$ in Eq. (26)):

Ψ 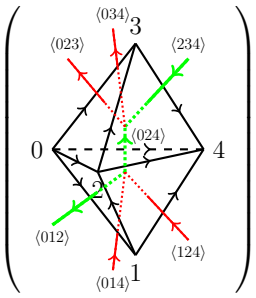

$= F(g_0,g_1,g_2,g_3,g_4)\ \Psi$ 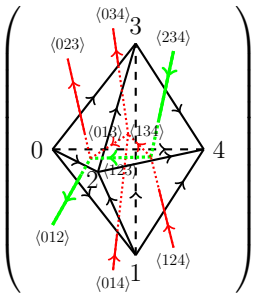

, (25)

Ψ 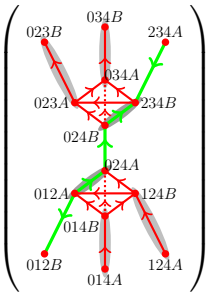

$= F(g_0,g_1,g_2,g_3,g_4)\ \Psi$ 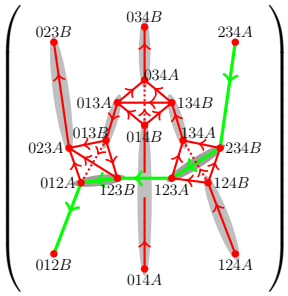

, (26)

where the F operator is given by

$$F(g_0,g_1,g_2,g_3,g_4)=\nu_4(g_0,g_1,g_2,g_3,g_4)c_{(0124)}^{\dagger n_3(0124)}c_{(0234)}^{\dagger n_3(0234)}c_{(0123)}^{n_3(0123)}c_{(0134)}^{n_3(0134)}c_{(1234)}^{n_3(1234)}X[\tilde{n}_2(g_i,g_j,g_k)]. \tag{27}$$

Here, $c_{(0124)}^{\dagger n_3(0124)}$ is the abbreviation of $c_{(0124)}^{\dagger n_3(g_0,g_1,g_2,g_4)}$ which is the creation operator for c fermion at tetrahedron $\langle 0124\rangle$, etc. The $X[\tilde{n}_2]$ operator in the above F move from the resolved dual lattice $\tilde{\mathcal{P}}$ to $\tilde{\mathcal{P}}'$ has the following general expression:

$$X[\tilde{n}_2(g_i,g_j,g_k)]=P_{\tilde{\mathcal{P}}}\cdot\gamma_{012A}^{\tilde{n}_2^2(g_0,g_1,g_2,g_3,g_4)},$$
$$P_{\tilde{\mathcal{P}}}=\left(\prod_{\text{loop } i \text{ in } (\tilde{\mathcal{P}},\tilde{\mathcal{P}}')}2^{(n_i-1)/2}\right)\left(\prod_{\text{Majorana pairs } \langle a,b\rangle \text{ in } \tilde{\mathcal{P}}}P_{a,b}\right)\left(\prod_{\text{link } \langle ijk\rangle\notin\tilde{\mathcal{P}}}P_{ijkA,ijkB}\right), \tag{28}$$

where $2n_i$ is the length of the i-th loop in the transition graph of dimer configurations in $\tilde{\mathcal{P}}$ and $\tilde{\mathcal{P}}'$. $P_{a,b}=(1-i\gamma_a\gamma_b)/2$ is the projection operator for Majorana pairs $\langle a,b\rangle$ (from vertex a to vertex b). The projection operators in the second parenthesis project the state in the right figure to the Majorana dimer configuration states in the left figure. The projection operators in the third parenthesis are the vacuum projection operators for those Majorana fermions that do not appear in the left figure explicitly (this is similar to the projection $P_{02A,02B}$ in Eq. (11) of the 2D case). An explicit expression of X for the Majorana pair configuration in Eqs. (25) and (26) is

$$X[\tilde{n}_2]=2\left(P_{024B,234B}P_{012A,024A}\right)\left(P_{013A,013B}P_{123A,123B}P_{134A,134B}\right)\gamma_{012A}. \tag{29}$$

When the F move changes the Majorana fermion parity, the last term of X operator is the Majorana fermion operator $\gamma_{012A} = a_{(012)} + a^\dagger_{(012)}$. The X operator is now an operator with odd number of a fermion creation or annihilation operators, and indeed changes the fermion parity of the state. We have checked that, for all possible Kitaev's Majorana chain configurations, the loop breaking Kasteleyn orientation in the transition graph of the two Majorana dimer states always contains the vertex $012A$. Therefore the X operator with γ_{012A} will indeed project the state to the desired Majorana configuration state (not 0). In fact, γ_{234B} is also an allowed choice. We will calculate the consistent equation of ν_4 for both choices later.

The fermionic local unitary transformation F should also be G_b symmetric:

$$F(g_0, g_1, g_2, g_3, g_4) = F(gg_0, gg_1, gg_2, gg_3, gg_4), \tag{30}$$

for all $g \in G_b$ if G_b is a unitary symmetry group. So $\nu_4(g_0, g_1, g_2, g_3, g_4)$, $n_3(g_0, g_1, g_2, g_3)$ and $\tilde{n}_2(g_0, g_1, g_2)$ are all cochains that are invariant under unitary g action. (We note that $\nu_4(gg_0, gg_1, gg_2, gg_3, gg_4) = \nu_4^*(g_0, g_1, g_2, g_3, g_4)$ for antiunitary g action.)

Similar to the 2D case, we can also change the phase factor ν_4 in the F operator to

$$\nu_4'(g_0, g_1, g_2, g_3, g_4) = \nu_4(g_0, g_1, g_2, g_3, g_4) \frac{\mu_3(g_1, g_2, g_3, g_4)\mu_3(g_0, g_1, g_3, g_4)\mu_3(g_0, g_1, g_2, g_3)}{\mu_3(g_0, g_2, g_3, g_4)\mu_3(g_0, g_1, g_2, g_4)} (-1)^{Sq^2(m_2)(g_0, g_1, g_2, g_3, g_4)}, \tag{31}$$

where $\mu_3(g_0, g_1, g_2, g_3)$ is a $U_T(1)$-valued 3-cochain, $m_2(g_0, g_1, g_2)$ is a $\mathbb{Z}_2$-valued 2-cocycle. $m_2 = 0, 1$ indicates the decoration of another complex fermions on the triangular faces of $\mathcal{T}$. The two fixed-point states can be smoothly connect by a FSLU transformation U_{μ_3, m_2}, which is given by

$$U_{\mu_3, m_2} |\{g_n\}\rangle = \prod_{\langle ijkl\rangle} \mu_3(g_i, g_j, g_k, g_l)^{s_{\langle ijkl\rangle}} \prod_{\langle ijk\rangle} f^{\dagger m_2(g_i, g_j, g_k)}_{(ijk)} |\{g_n\}\rangle, \tag{32}$$

where $s_{\langle ijkl\rangle} = \pm 1$ is the orientation of the tetrahedron $\langle ijkl\rangle$, and $f_{(ijk)}$ is the annihilation operator of the new fermions decorated on the triangle $\langle ijk\rangle$. Therefore, elements ν_4 in the rigid quotient group $H^4_{\text{rigid}}(G_b, U_T(1)) = H^4(G_b, U_T(1))/\Gamma$ correspond to the same 3D FSPT phase [42]. Here Γ is the subgroup of $H^4(G_b, U_T(1))$ generated by $(-1)^{Sq^2(m_2)}$.

Besides the standard (2-3) move, there are also (2-0) moves as unitary conditions. One example of the Majorana fermion configuration for (2-0) move is:

$$\Psi \left(\quad \right) = c^{\dagger n_3(g_0, g_1, g_2, g_3)}_{(0123)} \bar{c}^{\dagger n_3(g_0, g_1, g_2, g_3)}_{(0123)} X[\tilde{n}_2(g_i, g_j, g_k)] \; \Psi \left(\quad \right), \tag{33}$$

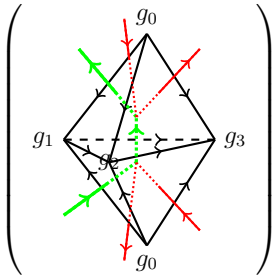

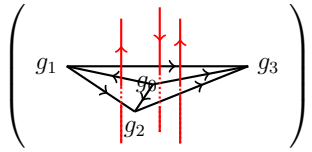

$$\Psi \left(\quad \right) = c^{\dagger n_3(g_0, g_1, g_2, g_3)}_{(0123)} \bar{c}^{\dagger n_3(g_0, g_1, g_2, g_3)}_{(0123)} X[\tilde{n}_2(g_i, g_j, g_k)] \; \Psi \left(\quad \right). \tag{34}$$

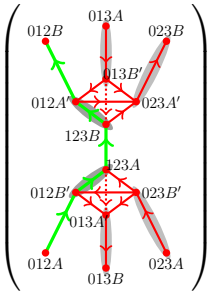

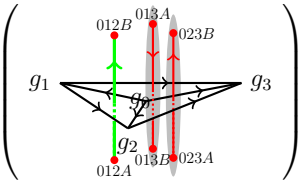

The notations and conventions of vacuum pairs are similar to the 2D case in the discussion below Eq. (15). An explicit expression for X operator is

$$X[\tilde{n}_2] = 2^{3/2} P_{123B, 012A'} P_{012B', 123A} P_{013A, 013B'} P_{023A', 023B} P_{013A, 013B} P_{023A, 023B'}. \tag{35}$$

Using the unitary conditions, we can deduce all (1-4) moves and other (2-3) moves from the standard F move in Eqs. (25) and (26).

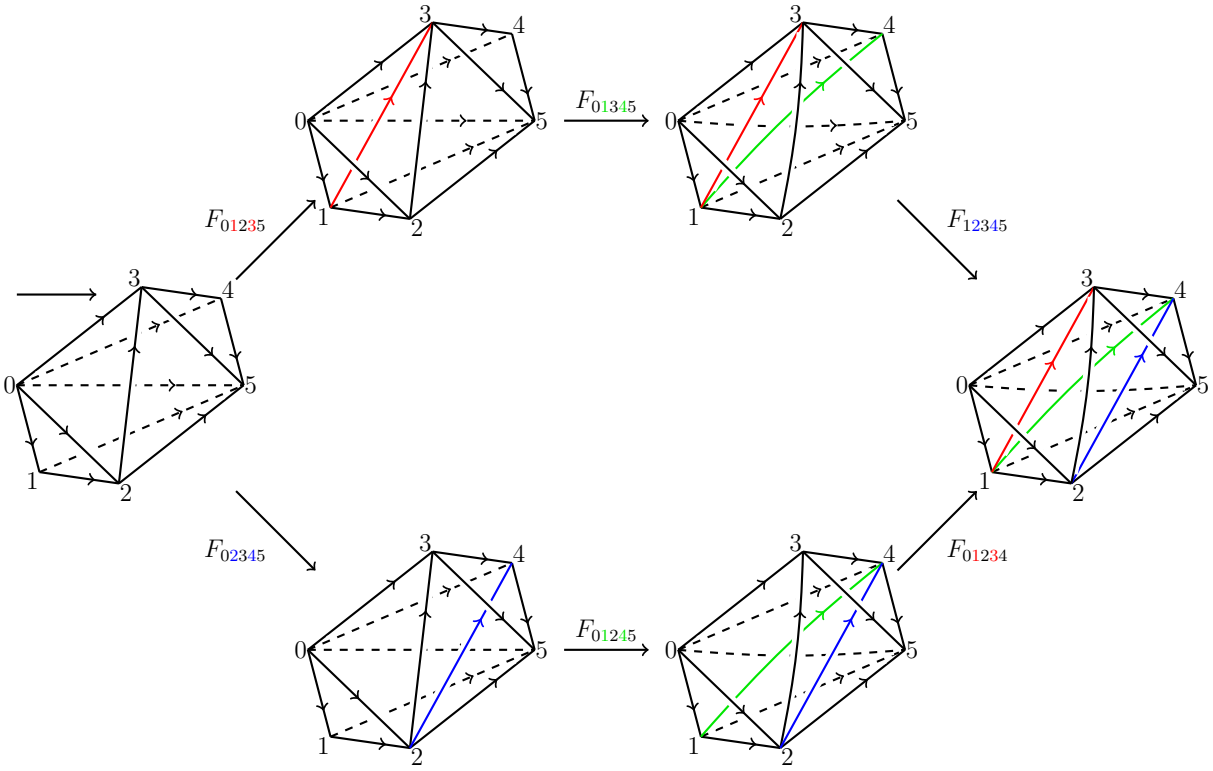

FIG. 19: Fermionic fusion hexagon equation. All the F moves are of the standard (2-3) move (see Fig. 25 and Fig. 26). Colored numbers i and j in the subscript of F indicate that the link $\langle ij\rangle$ with the same color is added after this F move. All the six F moves do not introduce new singular lines and surfaces. There is a global time direction from left to right such that the vertex with smaller number has earlier time.

3. *Fermionic hexagon equation*

The consistent equation for the moves defined in the above subsection is the fermionic hexagon equation (see Fig. 19), which is a higher dimensional version of the fermionic pentagon equation for (2+1)D fermionic topological phases [61]. Reordering the fermionic operators in the fermionic hexagon equation will twist the bosonic cocycle equation for ν_4:

$$(\mathrm{d}\nu_4)(g_0,g_1,g_2,g_3,g_4,g_5)=\mathcal{O}(g_0,g_1,g_2,g_3,g_4,g_5). \tag{36}$$

The phase twist or obstruction on the left-hand side has three terms

$$\mathcal{O}=\mathcal{O}_c\mathcal{O}_{c\gamma}\mathcal{O}_\gamma, \tag{37}$$

resulting from three different fermion phase factor: (1) $\mathcal{O}_c$ from reordering c fermions, (2) $\mathcal{O}_{c\gamma}$ from reordering c fermions and γ Majorana fermions, (3) $\mathcal{O}_\gamma$ from reordering γ Majorana fermions. The final result of phase twist is

$$\begin{aligned}\mathcal{O}(012345)=(-1)^{(n_3\smile_1 n_3)(012345)+(n_3\smile_2 \mathrm{d}n_3)(012345)+\mathrm{d}n_3(02345)\mathrm{d}n_3(01245)\mathrm{d}n_3(01234)}\\ \cdot i^{\mathrm{d}n_3(01235)\mathrm{d}n_3(02345)+\mathrm{d}n_3(01345)\mathrm{d}n_3(12345)}\cdot(-i)^{\mathrm{d}n_3(02345)\mathrm{d}n_3(01245)+\mathrm{d}n_3(02345)\mathrm{d}n_3(01234)}.\end{aligned} \tag{38}$$

Here, (012345) is the abbreviation of $(g_0,g_1,g_2,g_3,g_4,g_5)$, etc. Note that the obstruction only depends on n_3 and $\mathrm{d}n_3$ (or $\tilde{n}_2^2$ through the fermion parity equation $\mathrm{d}n_3=\tilde{n}_2^2$). In the following, we will derive the above obstruction equation in detail.

The first part $\mathcal{O}_c$ contains the (special) group super-cohomology result [42], which is obtained by reordering c fermion operators:

$$\begin{aligned}\mathcal{O}_c(012345)&=(-1)^{\left[Sq^2(n_3)+\mathrm{d}n_3\smile_2 n_3\right](012345)}=(-1)^{[n_3\smile_1 n_3+\mathrm{d}n_3\smile_2 n_3](012345)}\\ &=(-1)^{n_3(0345)n_3(0123)+n_3(0145)n_3(1234)+n_3(0125)n_3(2345)}\\ &\quad\cdot(-1)^{\mathrm{d}n_3(01234)n_3(0145)+\mathrm{d}n_3(02345)n_3(0125)+\mathrm{d}n_3(01234)n_3(1245)+\mathrm{d}n_3(01345)n_3(1235)+\mathrm{d}n_3(01234)n_3(2345)+\mathrm{d}n_3(01245)n_3(2345)}.\end{aligned} \tag{39}$$

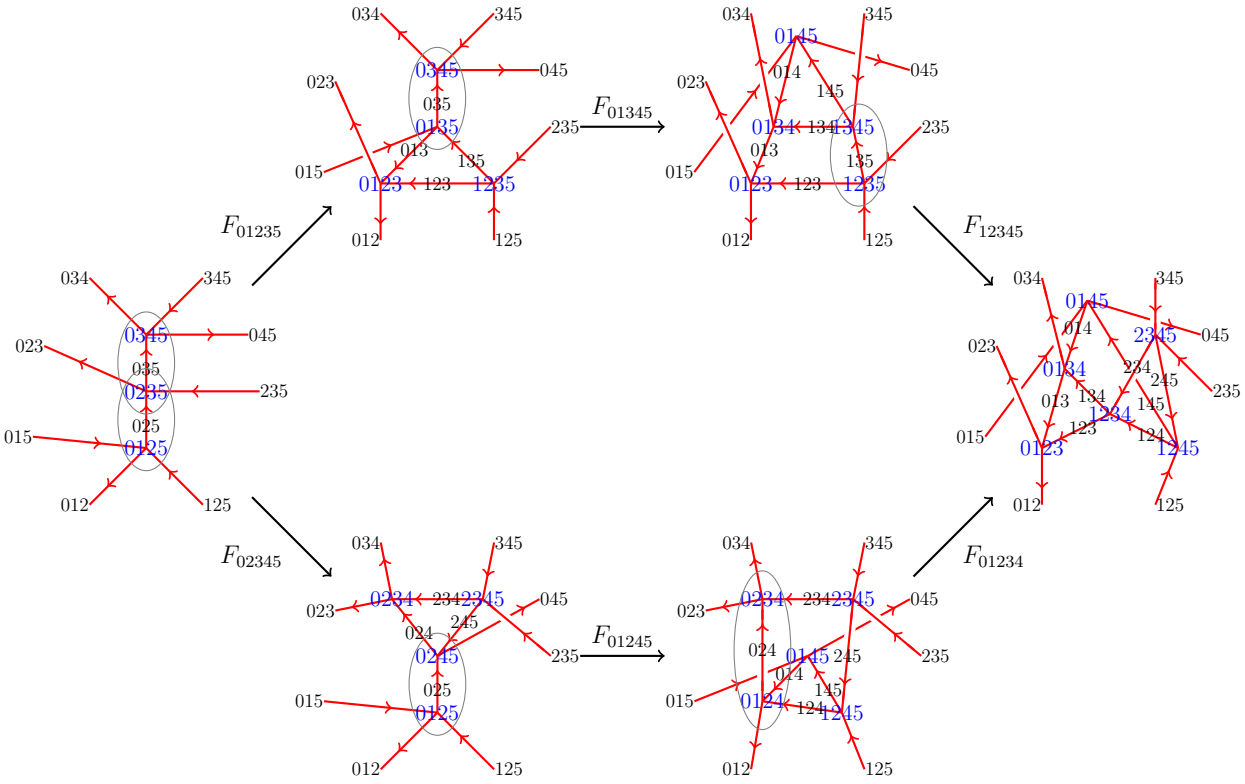

FIG. 20: Fermionic fusion hexagon equation on dual lattice $\mathcal{P}$.

Here, $\smile_i$ is the Steenrod's i-th cup product [72]. Apart from the term $Sq^2(n_3)$, there is an additional term $\mathrm{d}n_3 \smile_2 n_3$ because of $\mathrm{d}n_3 = \tilde{n}_2^2 \neq 0$.

The second part $\mathcal{O}_{c\gamma}$ comes from reordering c fermions and γ Majorana fermions (we always putting c fermions in front of γ fermions). For example, the composition of F_{01345} and F_{01235} gives a sign $(-1)^{\mathrm{d}n_3(01345)\mathrm{d}n_3(01235)}$. In total, the upper path of three F moves gives the power $\mathrm{d}n_3(01345)\mathrm{d}n_3(01235) + \mathrm{d}n_3(12345)\mathrm{d}n_3(01345) + \mathrm{d}n_3(12345)\mathrm{d}n_3(01235)$, while the lower path gives $\mathrm{d}n_3(01245)\mathrm{d}n_3(01234)+\mathrm{d}n_3(02345)\mathrm{d}n_3(01234)+\mathrm{d}n_3(02345)\mathrm{d}n_3(01245)$. The final result is then

$$\mathcal{O}_{c\gamma}(012345) = (-1)^{(\mathrm{d}n_3 \smile_3 \mathrm{d}n_3)(g_0,g_1,g_2,g_3,g_4,g_5)} \tag{40}$$
$$= (-1)^{\mathrm{d}n_3(01245)\mathrm{d}n_3(01234)+\mathrm{d}n_3(01235)\mathrm{d}n_3(01345)+\mathrm{d}n_3(02345)\mathrm{d}n_3(01234)+\mathrm{d}n_3(02345)\mathrm{d}n_3(01245)+\mathrm{d}n_3(01235)\mathrm{d}n_3(12345)+\mathrm{d}n_3(01345)\mathrm{d}n_3(12345)}.$$

After adding a cochain $(-1)^{\mathrm{d}(n_3 \smile_3 \mathrm{d}n_3)} = (-1)^{\mathrm{d}n_3 \smile_3 \mathrm{d}n_3 + n_3 \smile_2 \mathrm{d}n_3 + \mathrm{d}n_3 \smile_2 n_3}$ to the combination of the phase factor $\mathcal{O}_c$ and $\mathcal{O}_{c\gamma}$, we get a simpler expression

$$\mathcal{O}_c\mathcal{O}_{c\gamma} = (-1)^{n_3 \smile_1 n_3 + n_3 \smile_2 \mathrm{d}n_3}. \tag{41}$$

Now let us turn to the subtlest part $\mathcal{O}_\gamma$ coming from decorated Majorana chain. Besides ± 1, $\mathcal{O}_\gamma$ can also takes value in $\pm i$. If all the six F moves do not change the Majorana fermion parity, then X_γ operators in F moves are merely projections with even number of γ Majorana operators. The c fermions and Majorana fermions are decoupled, and both $\mathcal{O}_{c\gamma}$ and $\mathcal{O}_\gamma$ are trivial. The obstruction $\mathcal{O}$ is the same as the (special) group super-cohomology result. Therefore, we only need to check the case that some of the six F moves in Fig. 19 change the Majorana fermion parity, i.e., some of $\tilde{n}_2^2(01234)$, $\tilde{n}_2^2(01245)$, $\tilde{n}_2^2(02345)$, $\tilde{n}_2^2(01345)$, $\tilde{n}_2^2(01235)$ and $\tilde{n}_2^2(12345)$ equal to one. Let us denote the six X operators in F moves as $X_{01235} = P_1\gamma_{012A}^{\tilde{n}_2^2(01235)}$, $X_{01345} = P_2\gamma_{013A}^{\tilde{n}_2^2(01345)}$, $X_{12345} = P_3\gamma_{123A}^{\tilde{n}_2^2(12345)}$, $X_{02345} = P_1\gamma_{023A}^{\tilde{n}_2^2(02345)}$, $X_{01245} = P_4\gamma_{012A}^{\tilde{n}_2^2(01245)}$, $X_{01234} = P_5\gamma_{012A}^{\tilde{n}_2^2(01234)}$. Here, P_i means the projection operator onto the Majorana chain configuration of the i-th figure in the hexagon equation. $\mathcal{O}_\gamma$ is defined as the Majorana chain phase difference of the upper and lower paths in hexagon equation

$$X_{02345}X_{01245}X_{01234}|\mathrm{final}\rangle = \mathcal{O}_\gamma(012345)X_{01235}X_{01345}X_{12345}|\mathrm{final}\rangle, \tag{42}$$

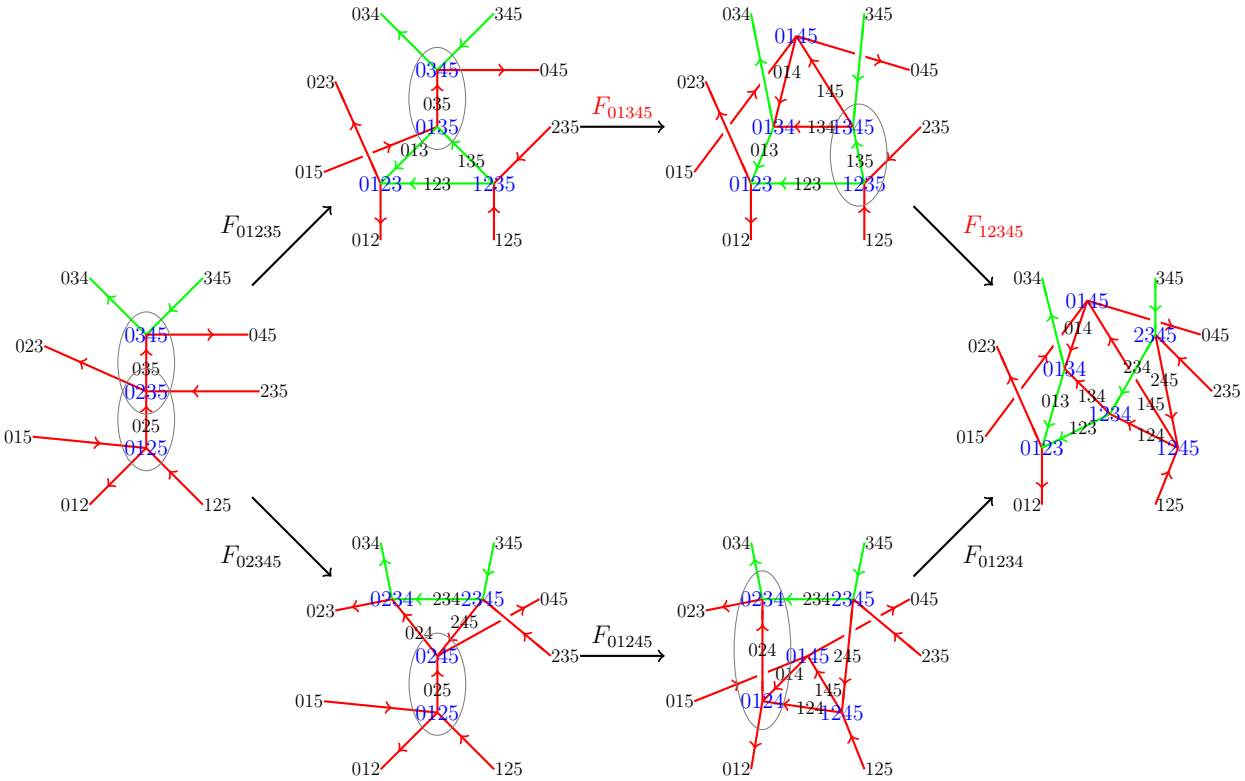

FIG. 21: One example of Kitaev's Majorana chain decoration configuration of fermionic fusion hexagon equation. Green lines indicate that these dual links are decorated by Kitaev's Majorana chains. Among the six F moves for this configuration, only F_{01345} and F_{12345} (red color in the figure) change the Majorana fermion parity. Therefore this choice of $\tilde{n}_2(g_i, g_j, g_k)$ belongs to the $(0, 1, 1, 0, 0, 0)$ row in Table II and has obstruction $\mathcal{O}_\gamma = i$.

where $|\text{final}\rangle$ is the state of Majorana chain configuration in the rightmost figure of the hexagon equation Fig. 20. We can calculate $\mathcal{O}_\gamma$ from the expression

$$\begin{aligned}\mathcal{O}_\gamma(012345) &= \langle \text{final}| X^\dagger_{12345} X^\dagger_{01345} X^\dagger_{01235} X_{02345} X_{01245} X_{01234} |\text{final}\rangle \\ &= \langle \text{final}| \gamma_{123A}^{\tilde{n}_2^2(12345)} P_3 \gamma_{013A}^{\tilde{n}_2^2(01345)} P_2 \gamma_{012A}^{\tilde{n}_2^2(01235)} P_1 P_1 \gamma_{023A}^{\tilde{n}_2^2(02345)} P_4 \gamma_{012A}^{\tilde{n}_2^2(01245)} P_5 \gamma_{012A}^{\tilde{n}_2^2(01234)} |\text{final}\rangle. \end{aligned} \tag{43}$$

The above equation suggests that $\mathcal{O}_\gamma$ depends only on the values of $\tilde{n}_2^2(01235)$, $\tilde{n}_2^2(01345)$, $\tilde{n}_2^2(12345)$, $\tilde{n}_2^2(02345)$, $\tilde{n}_2^2(01245)$, and $\tilde{n}_2^2(01234)$, i.e., the Majorana parity changes of the six F moves.

Consider, for example, the case where only F_{01345} and F_{12345} change the Majorana fermion parity [$(0, 1, 1, 0, 0, 0)$ in the eighth row of Table II. See also Fig. 21 for an example of $\tilde{n}_2(g_i, g_j, g_k)$ satisfying this condition]. We can expand projection operators P_i to Majorana fermion operators. For simplicity, we can consider the term with only contributions $-i\gamma_{013A}\gamma_{013B}$ and $-i\gamma_{123A}\gamma_{123B}$ from P_1. We can also add $-i\gamma_{013B}\gamma_{123B}$ which equals to 1 when acting on $|\text{final}\rangle$ in front of this state. The result is then

$$\begin{aligned}\mathcal{O}_\gamma(012345)|_{(0,1,1,0,0,0)} &= \langle \text{final}|\gamma_{123A} P_3 \gamma_{013A} P_2 P_1 P_4 P_5 P_6 |\text{final}\rangle \\ &= \langle \text{final}|\gamma_{123A}\gamma_{013A}(-i\gamma_{013A}\gamma_{013B})(-i\gamma_{123A}\gamma_{123B})(-i\gamma_{013B}\gamma_{123B})|\text{final}\rangle \\ &= i. \end{aligned} \tag{44}$$

We have assumed that there are only two Kitaev strings meeting at at tetrahedron $\langle 0123\rangle$ (we find this is always true for all possible choices $\tilde{n}_2(g_i, g_j, g_k)$ that belong to the eighth row of Table II). Similarly, one can calculate other choices of $\tilde{n}_2$, and at last obtain the results listed in Table II. The final results can be summarized to an expression

$$\mathcal{O}_\gamma(012345) = i^{\tilde{n}_2^2(01235)\tilde{n}_2^2(02345)+\tilde{n}_2^2(01345)\tilde{n}_2^2(12345)} (-i)^{\tilde{n}_2^2(02345)\tilde{n}_2^2(01245)+\tilde{n}_2^2(02345)\tilde{n}_2^2(01234)} (-1)^{\tilde{n}_2^2(02345)\tilde{n}_2^2(01245)\tilde{n}_2^2(01234)}. \tag{45}$$

Combining this $\mathcal{O}_\gamma$ result with $\mathcal{O}_c\mathcal{O}_{c\gamma}$ in Eq. (41), we obtain the obstruction claimed in Eq. (38).

TABLE II: Calculations of $\mathcal{O}_\gamma$ from all possible Kitaev chain configurations in hexagon equation. The first column has entry $\big(\tilde{n}_2^2(01235), \tilde{n}_2^2(01345), \tilde{n}_2^2(12345), \tilde{n}_2^2(02345), \tilde{n}_2^2(01245), \tilde{n}_2^2(01234)\big)$, indicating whether the six F moves in the hexagon equation change the Majorana fermion parity or not. The second column shows the γ operators appearing in Eq. (43). The third and fourth columns are lines of Majorana dimer pairs ($\emptyset$ means there are no $\tilde{n}_2(g_i, g_j, g_k)$ that has 2 or 4 strings at tetrahedron $\langle 0123\rangle$). The last column is the value of $\mathcal{O}_\gamma$ for $\tilde{n}_2(g_i, g_j, g_k)$ belongs to this row. Nontrivial results are labelled by red color. The results in this table can be summarized to an expression shown in Eq. (45).

fermion parity changes	γ operators in Eq. (43)	line (2 strings at $\langle 0123\rangle$)	line (4 strings at $\langle 0123\rangle$)	$\mathcal{O}_\gamma$
$(0,0,0,0,0,0)$	–	–	–	1
$(1,1,0,0,0,0)$	$\gamma_{012A}, \gamma_{013A}$	$012A$-$013B$-$013A$	$\emptyset$	1
$(1,0,1,0,0,0)$	$\gamma_{012A}, \gamma_{123A}$	$012A$-$123B$-$123A$	$\emptyset$	1
$(1,0,0,1,0,0)$	$\gamma_{012A}, \gamma_{023A}$	$012A$-$023A$	$\emptyset$	i
$(1,0,0,0,1,0)$	$\gamma_{012A}^2 = 1$	–	–	1
$(1,0,0,0,0,1)$	$\gamma_{012A}^2 = 1$	–	–	1
$(0,1,1,0,0,0)$	$\gamma_{013A}, \gamma_{123A}$	$013A$-$013B$-$123B$-$123A$	$\emptyset$	i
$(0,1,0,1,0,0)$	$\gamma_{013A}, \gamma_{023A}$	$013A$-$013B$-$023A$	$\emptyset$	1
$(0,1,0,0,1,0)$	$\gamma_{013A}, \gamma_{012A}$	$013A$-$013B$-$012A$	$\emptyset$	1
$(0,1,0,0,0,1)$	$\gamma_{013A}, \gamma_{012A}$	$013A$-$013B$-$012A$	$\emptyset$	1
$(0,0,1,1,0,0)$	$\gamma_{123A}, \gamma_{023A}$	$123A$-$123B$-$023A$	$\emptyset$	1
$(0,0,1,0,1,0)$	$\gamma_{123A}, \gamma_{012A}$	$123A$-$123B$-$012A$	$\emptyset$	1
$(0,0,1,0,0,1)$	$\gamma_{123A}, \gamma_{012A}$	$123A$-$123B$-$012A$	$\emptyset$	1
$(0,0,0,1,1,0)$	$\gamma_{023A}, \gamma_{012A}$	$023A$-$012A$	$\emptyset$	$-i$
$(0,0,0,1,0,1)$	$\gamma_{023A}, \gamma_{012A}$	$023A$-$012A$	$\emptyset$	$-i$
$(0,0,0,0,1,1)$	$\gamma_{012A}^2 = 1$	–	–	1
$(1,1,0,0,1,1)$	$\gamma_{013A}, \gamma_{012A}^3$	$012A$-$013B$-$013A$, $012A$	$\emptyset$	1
$(1,0,1,0,1,1)$	$\gamma_{123A}, \gamma_{012A}^3$	$012A$-$123B$-$123A$, $012A$	$\emptyset$	1
$(1,0,0,1,1,1)$	$\gamma_{023A}, \gamma_{012A}^3$	$012A$-$023A$, $012A$	$\emptyset$	i
$(1,1,1,1,0,0)$	$\gamma_{012A}, \gamma_{013A}, \gamma_{123A}, \gamma_{023A}$	$\emptyset$	$123A$-$123B$-$013B$-$013A$ $023A$-$012A$	-1
$(0,1,1,1,1,0)$	$\gamma_{013A}, \gamma_{123A}, \gamma_{023A}, \gamma_{012A}$	$\emptyset$	$123A$-$123B$-$013B$-$013A$ $023A$-$012A$	1
$(0,1,1,1,0,1)$	$\gamma_{013A}, \gamma_{123A}, \gamma_{023A}, \gamma_{012A}$	$\emptyset$	$123A$-$123B$-$013B$-$013A$ $023A$-$012A$	1
$(1,1,1,1,1,1)$	$\gamma_{013A}, \gamma_{123A}, \gamma_{023A}, \gamma_{012A}^3$	$\emptyset$	$123A$-$123B$-$013B$-$013A$ $023A$-$012A$	-1

As discussed above, we can also use the convention $X_{01234} = P_{\mathcal{P}} \gamma_{234B}^{\tilde{n}_2^2(01234)}$ in the definition of standard F move. The obstruction from Majorana fermion in this convention is

$$\mathcal{O}_\gamma(012345) = i^{\tilde{n}_2^2(01235)\tilde{n}_2^2(02345)+\tilde{n}_2^2(01245)\tilde{n}_2^2(01234)} (-i)^{\tilde{n}_2^2(01235)\tilde{n}_2^2(01345)+\tilde{n}_2^2(01235)\tilde{n}_2^2(12345)} (-1)^{\tilde{n}_2^2(01235)\tilde{n}_2^2(01345)\tilde{n}_2^2(12345)}. \tag{46}$$

We note that although $\mathcal{O}$ takes value on $\mathbb{Z}_4$, the additivity property actually requires $\mathcal{O}$ to be a cohomology map on $\mathbb{Z}_8$, see Appendix C for details. Thus, we see that in order to find a solution for ν_4, we must define an obstruction free subgroup of $H^2(G_b, \mathbb{Z}_2)$, which is formed by elements $\tilde{n}_2 \in H^2(G_b, \mathbb{Z}_2)$ that simultaneously satisfy $Sq^2(\tilde{n}_2) = 0$ in $H^4(G_b, \mathbb{Z}_2)$ and $\mathcal{O}(\tilde{n}_2) = 0$ in $H^5(G_b, U_T(1))$, where $\mathcal{O}$ is some unknown cohomology operation (to the best of our knowledge) that maps $\tilde{n}_2$ satisfying $Sq^2(\tilde{n}_2) = 0$ in $H^2(G_b, \mathbb{Z}_2)$ into an element in $H^5(G_b, \mathbb{Z}_8) \subset H^5[G_b, U_T(1)]$. We note that n_3 is completely determined by $\tilde{n}_2$ and any solution of $dn_3 = \tilde{n}_2^2$ can be used in the above definition. Together with the special group super-cohomolgy results, we conclude that the precise mathematical objects that classify 3D FSPT phases with a total symmetry $G_f = G_b \times \mathbb{Z}_2^f$ can also be summarized as three group cohomologies of the symmetry group: $\tilde{B}H^2(G_b, \mathbb{Z}_2)$, $BH^3(G_b, \mathbb{Z}_2)$ and $H^4_{\text{rigid}}(G_b, U_T(1))$. Commuting projector parent Hamiltonians for all these FSPT states can also be constructed on all 3D triangulations(with a branching structure).

V. CONCLUSIONS AND DISCUSSIONS

In conclusion, we have constructed fixed point wavefucntions for FSPT states in 2D and 3D based on the novel concept of FSLU transformations. All these FSPT states admit parent Hamiltonians consisting of commuting projectors on arbitrary triangulations(with a branching structure). We believe that our construction will give rise to a complete classification for FSPT states with total symmetry $G_f = G_b \times \mathbb{Z}_2^f$ when G_b is a unitary symmetry group. Mathematically, our constructions naturally define a general group super-cohomology theory that generalizes the so-called special group super-cohomology theory proposed in Ref. 42.

In particular, one can start with a spin manifold in arbitrary spacial dimension d_{sp} and define the corresponding discrete spin structure via Poincare dual, then one can decorate Kitaev's Majorana chain on the intersection lines of G_b symmetry domain walls if the first obstruction vanishes for elements $\tilde{n}_{d_{sp}-1} \in H^{d_{sp}-1}(G_b, \mathbb{Z}_2)$. That is, $Sq^2(\tilde{n}_{d_{sp}+1}) = 0$ in $H^{d_{sp}+1}(G_b, \mathbb{Z}_2)$, and the obstruction free elements $\tilde{n}_{d_{sp}-1} \in H^{d_{sp}-1}(G_b, \mathbb{Z}_2)$ will give rise to all inequivalent pattern of Mjorana chain decoration. Finally, by applying the wavefunction renormalization on arbitrary triangulations, one may derive a twisted co-cycle equations where the twisted factors define some unknown cohomolgoy map $\mathcal{O}$ that maps elements in $H^{d_{sp}-1}(G_b, \mathbb{Z}_2)$ satisfying $Sq^2(\tilde{n}_{d_{sp}-1}) = 0$ in $H^{d_{sp}+1}(G_b, \mathbb{Z}_2)$ into elements in $H^{d_{sp}+2}(G_b, \mathbb{Z}_8) \subset H^{d_{sp}+2}[G_b, U_T(1)]$, and the second obstruction free condition requires $\mathcal{O}(\tilde{n}_{d_{sp}-1}) = 0$ in $H^{d_{sp}+2}(G_b, U_T(1))$. Elements $\tilde{n}_{d_{sp}-1} \in H^{d_{sp}-1}(G_b, \mathbb{Z}_2)$ satisfying both the first and second obstruction free conditions might define a subgroup $\tilde{B}H^{d_{sp}-1}(G_b, \mathbb{Z}_2) \in H^{d_{sp}-1}(G_b, \mathbb{Z}_2)$, which allows us to write down another short exact sequence $0 \to \mathcal{H}^{d_{sp}+1}[G_f, U_T(1)] \to H_f^{d_{sp}+1}[G_f, U_T(1)] \to \tilde{B}H^{d_{sp}-1}(G_b, \mathbb{Z}_2) \to 0$ to define a general group super-cohomology theory. We note that here $\mathcal{H}^{d_{sp}+1}[G_f, U_T(1)]$ is the special group super-cohomology class defined by Ref. 42.

For future work, it would be of great importance to understand the physical properties of 3D FSPT phases classified by general group super-cohomology theory, e.g. understanding the braiding statistics of G_b-flux lines. Of course, constructing time reversal symmetry protected FSPT states with both $T^2 = 1$ and $T^2 = P^f$ (where P^f is the total fermion parity) is another interesting direction. Moreover, it will also be interesting to investigate the phase transition theory among FSPT phases in arbitrary dimensions, which might define a new type of fractionalized string theory in arbitrary dimensions.

ACKNOWLEDGMENTS

We thank Zheng-Xin Liu and Jianwei Li for helpful discussions on solving system of linear Diophantine equations. We also thank Shuo Yang for the help of calculating these equations numerically. ZCG acknowledges start-up support, Direct Grant No. 4053163, No. 3132745 from The Chinese University of Hong Kong and the funding from RGC/ECS(No.2191110).

Note added – During the preparation of this work, we notice a relevant work Ref. 73 considering similar problems.

Appendix A: 2D Pachner moves

1. (2-2) moves

With branching structure, there are 3 different types of (2-2) Pachner moves. Only two of them can be induced by a global time ordering [see Eqs. (A1) and (A2)].

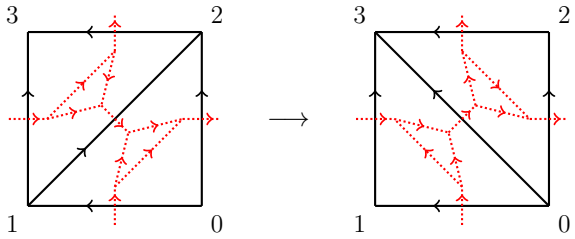

(A1)

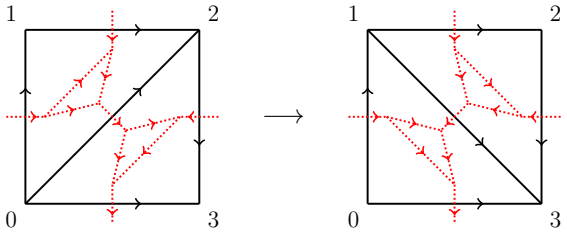

(A2)

Note that the (2-2) move in Eq. (A2) is the standard move in Fig. 8. The other (2-2) move in Eq. (A1) can be derive from a sequence of the standard move and the (2-0) moves in Eq. (15), as shown below:

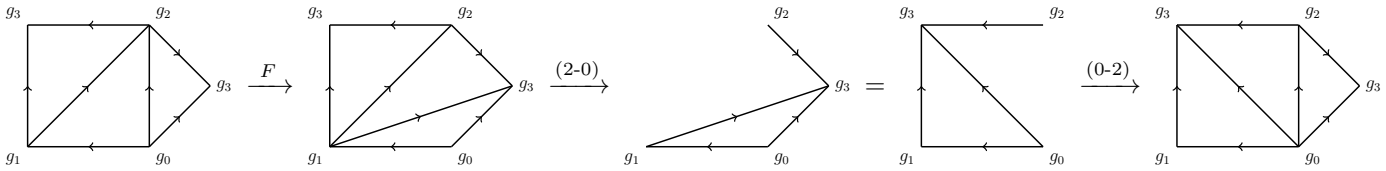

To derive the (2-2) move in Eq. (A1), we first add a vertex g_3 and a triangle labelled by g_0, g_2, g_3 on the right of the figure. The first step is a standard (2-2) F move. Then after a (2-0) move and a (0-2) move, we finally obtain the desired triangulation.

When decorating Kitaev's Majorana chains to the dual lattice, there are in total $2^3 = 8$ kinds of different decoration configurations (see Table III) for each (2-2) move. One can check that, for any decoration configuration, all the loops in the transition graph of the left and right Majorana dimer states have Kasteleyn orientation property. Therefore the Majorana fermion parity is conserved in all (2-2) moves.

out-leg string #	configuration
0	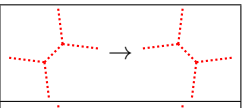
2	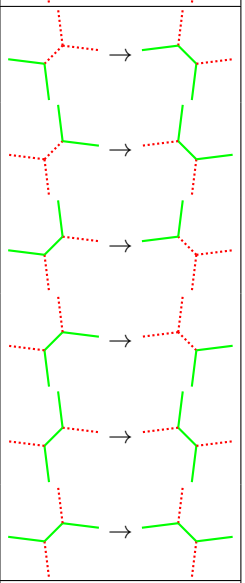
4	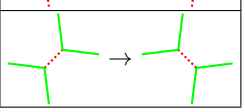

TABLE III: $2^3 = 8$ kinds of configurations of Kitaev's Majorana chain decorations (green line) on the dual lattice $\mathcal{P}$ for each (2-2) move.

2. (1-3) moves

There are in total 4 different types of (1-3) Pachner moves for triangulation with branching structure. Two of them have branching structure that can be induced by a global time ordering [see Eqs. (A3)-(A4)]. These (1-3) moves can also be derived from a sequence of the standard (2-2) move and (2-0) moves.

In total $2^3 = 8$ kinds of Kitaev's Majorana chain decoration configurations are summarized in Table IV. Similar to the (2-2) moves, one can check that all the (1-3) moves do not change the Majorana fermion parity for arbitrary decoration configurations.

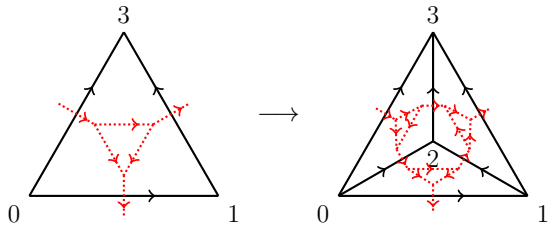

(A3)

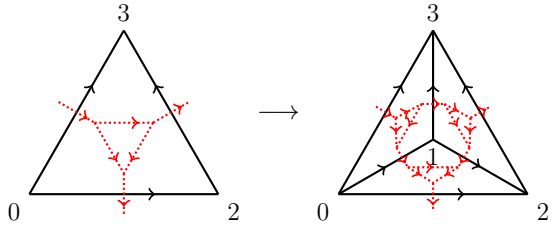

(A4)

out-leg string #	configuration-1	configuration-2
0	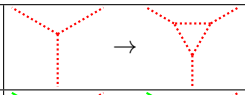	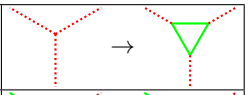
2	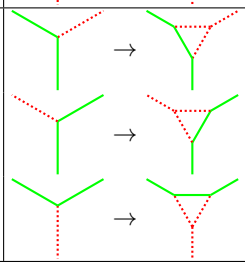	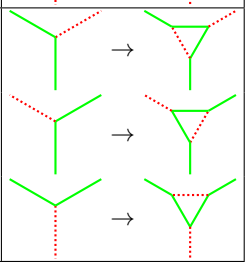

TABLE IV: $2^3 = 8$ kinds of configurations of Kitaev's Majorana chain decorations (green line) on the dual lattice $\mathcal{P}$ for each (1-3) move.

Appendix B: 3D Pachner moves and fermion parity changes

1. (2-3) moves

For 3D triangulation with branching structure, there are 10 different kinds of (2-3) Pachner moves. Eight of them have branching structure induced by global time ordering (see Figs. 22-29).

Note that the (2-3) move in Fig. 22 is the standard move in Fig. 15. Other (2-3) moves can be also derive from a sequence of the standard move and the (2-0) moves in Eq. (33). Here is an example of deriving the (inverse of) (2-3)

move in Fig. 26 from the standard move and (2-0) moves:

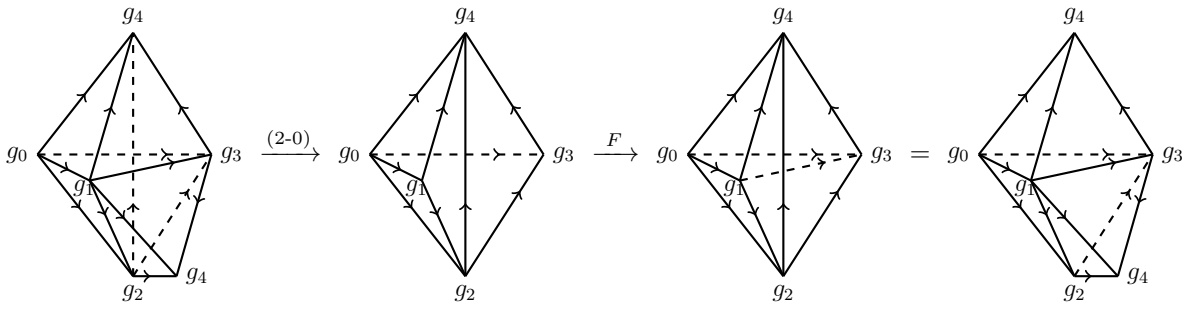

(B1)

We first add a vertex g_4 and a tetrahedron labelled by g_1, g_2, g_3, g_4 on the lower right of the figures on both side of Fig. 26. From the figure on the right hand side, we first perform a (2-0) move to remove the two tetrahedra labelled by g_1, g_2, g_3, g_4 but have opposite orientations. There are now only two tetrahedra left as shown in the second figure above. Now we can use the standard (2-3) F move to add a line connecting g_1 and g_3. The resulting figure (the third one) is the same as the last figure, after identifying the two vertices labelled by g_4. Therefore, the inverse of the (2-3) move in Fig. 26 is represented by a sequence of standard (2-3) move and (2-0) move.

Different from the 2D case, when decorating Kitaev's Majorana chains to the dual lattice, the (2-3) moves may change the Majorana fermion parity. One can check the Kasteleyn orientation property for all loops in the transition graph of the left and right Majorana dimer states. A striking result is that, for all the 10 kinds (2-3) moves, the move changes the Majorana fermion parity if and only if both link 012 and link 234 in lattice $\mathcal{P}$ are decorated by Kitaev's Majorana chains. This leads to the total fermion parity conservation equation $\mathrm{d}n_3 = \tilde{n}_2 \smile \tilde{n}_2$. $2^6 = 64$ kinds of Kitaev's Majorana chain decoration configurations are summarized in Table V.

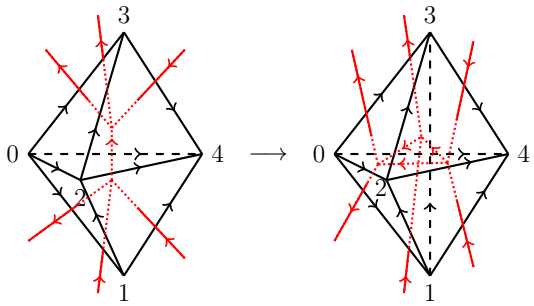

(a) For triangulation $\mathcal{T}$ and dual lattice $\mathcal{P}$.

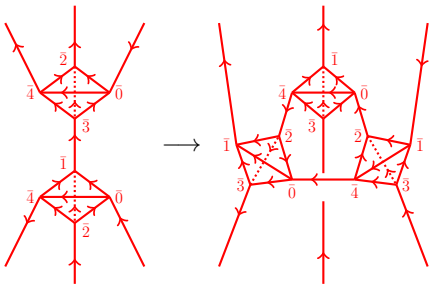

(b) For resolved dual lattice $\tilde{\mathcal{P}}$.

FIG. 22: (2-3)-A move.

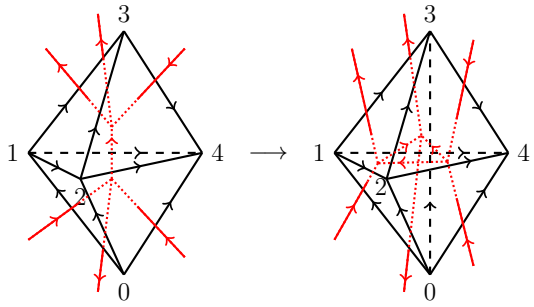

(a) For triangulation $\mathcal{T}$ and dual lattice $\mathcal{P}$.

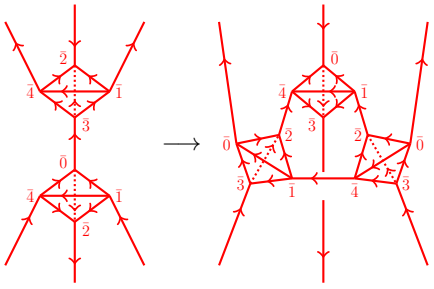

(b) For resolved dual lattice $\tilde{\mathcal{P}}$.

FIG. 23: (2-3)-B move.

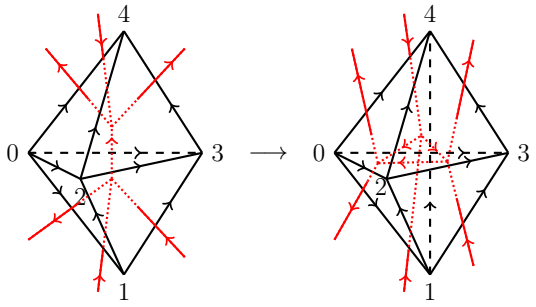

(a) For triangulation $\mathcal{T}$ and dual lattice $\mathcal{P}$.

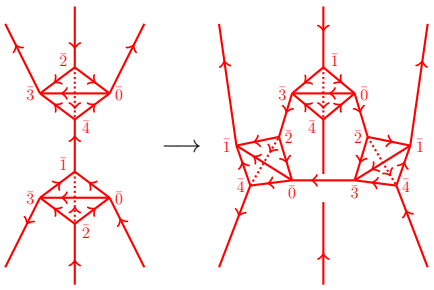

(b) For resolved dual lattice $\tilde{\mathcal{P}}$.

FIG. 24: (2-3)-C move.

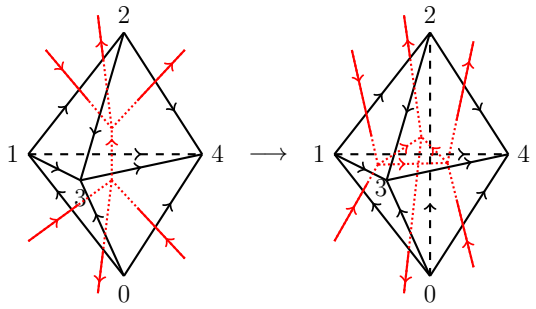

(a) For triangulation $\mathcal{T}$ and dual lattice $\mathcal{P}$.

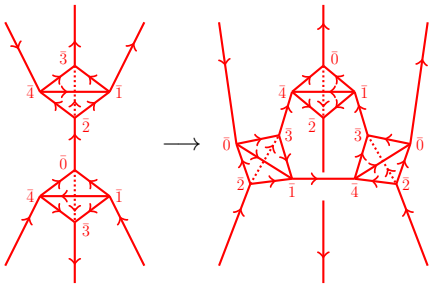

(b) For resolved dual lattice $\tilde{\mathcal{P}}$.

FIG. 25: (2-3)-D move.

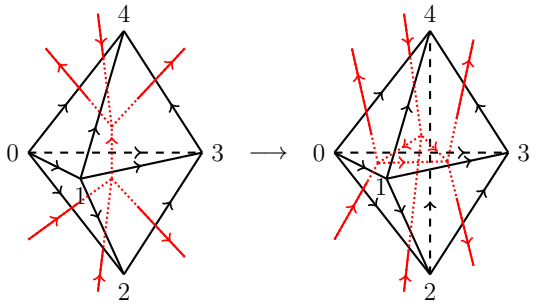

(a) For triangulation $\mathcal{T}$ and dual lattice $\mathcal{P}$.

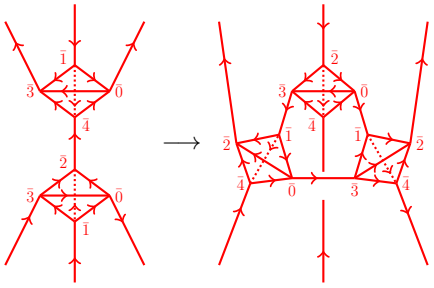

(b) For resolved dual lattice $\tilde{\mathcal{P}}$.

FIG. 26: (2-3)-E move.

2. (1-4) moves

There are 5 different kinds of (1-4) 3D Pachner moves. Three of them have branching structure that can be induced by global time ordering (see Figs. 30-32).

One can also check that, for all the 5 kinds (1-4) moves, the move changes the Majorana fermion parity if and only if both link 012 and link 234 in lattice $\mathcal{P}$ are decorated by Kitaev's Majorana chains. Therefore we also have $\mathrm{d}n_3 = \tilde{n}_2 \smile \tilde{n}_2$. $2^6 = 64$ kinds of Kitaev's Majorana chain decoration configurations are summarized in Table VI.

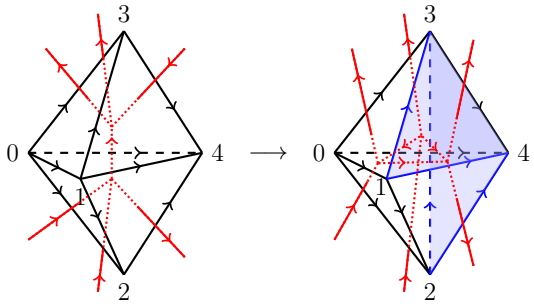

(a) For triangulation $\mathcal{T}$ and dual lattice $\mathcal{P}$.

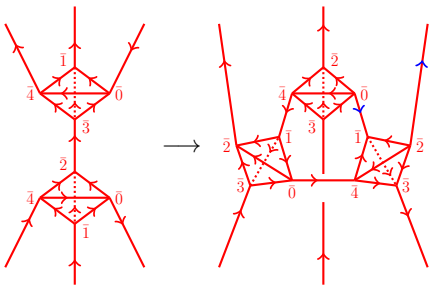

(b) For resolved dual lattice $\tilde{\mathcal{P}}$.

FIG. 27: (2-3)-F move.

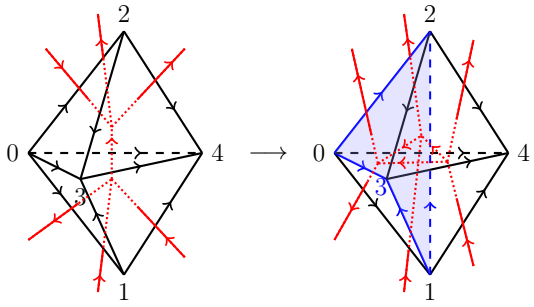

(a) For triangulation $\mathcal{T}$ and dual lattice $\mathcal{P}$.

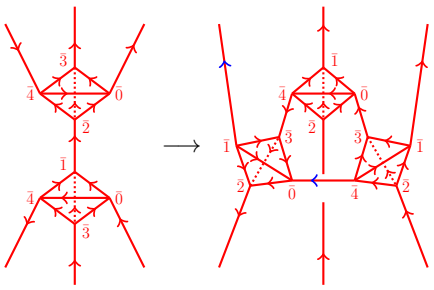

(b) For resolved dual lattice $\tilde{\mathcal{P}}$.

FIG. 28: (2-3)-G move.

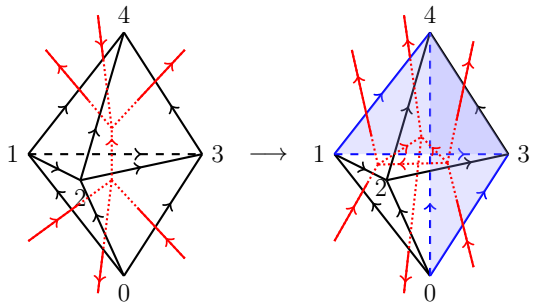

(a) For triangulation $\mathcal{T}$ and dual lattice $\mathcal{P}$.

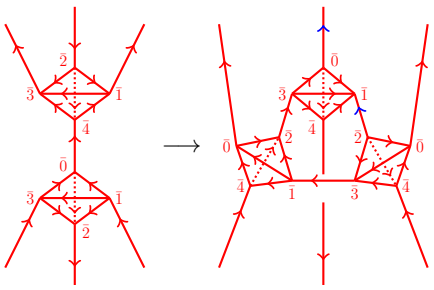

(b) For resolved dual lattice $\tilde{\mathcal{P}}$.

FIG. 29: (2-3)-H move.

out-leg string #	configuration #	configuration-1	configuration-2
0	1×2	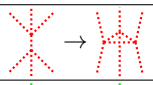	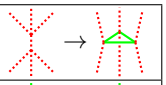
2	3×2	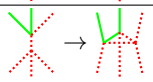	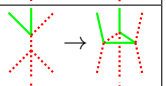
	3×2	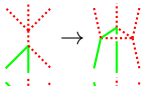	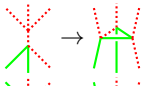
	3×2	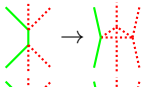	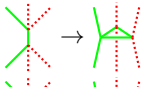
	6×2	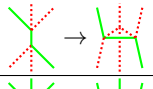	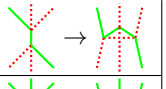
4	3×2	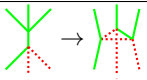	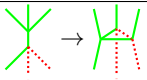
	3×2	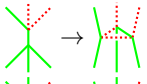	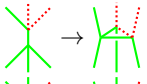
	3×2	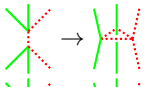	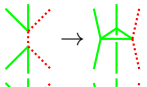
	6×2	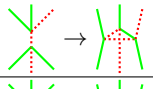	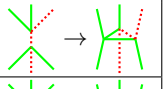
6	1×2	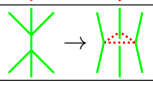	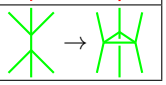

TABLE V: $2^6 = 64$ kinds of configurations of Kitaev's Majorana chain decorations (green line) on the dual lattice $\mathcal{P}$ for each (2-3) move. The second column counts the number of configurations of the same symmetry type. When four green lines meet at one point, we should resolve the decoration according to the conventions in Fig. 18.

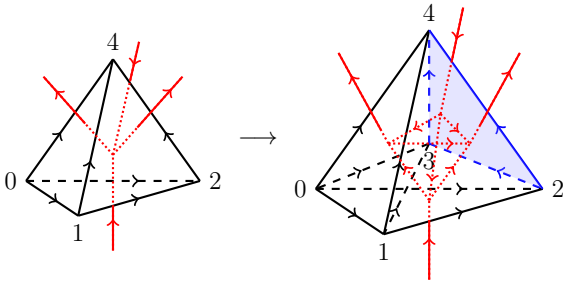

(a) For triangulation $\mathcal{T}$ and dual lattice $\mathcal{P}$.

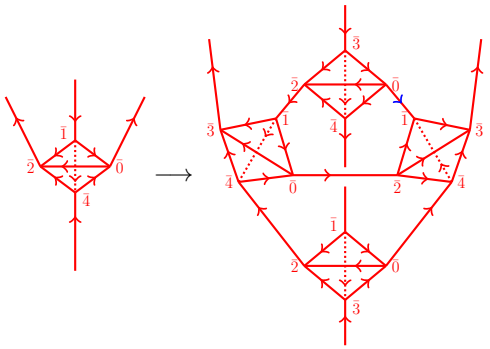

(b) For resolved dual lattice $\tilde{\mathcal{P}}$.

FIG. 30: (1-4)-A move.

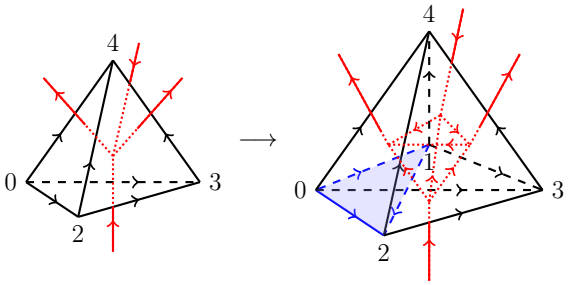

(a) For triangulation $\mathcal{T}$ and dual lattice $\mathcal{P}$.

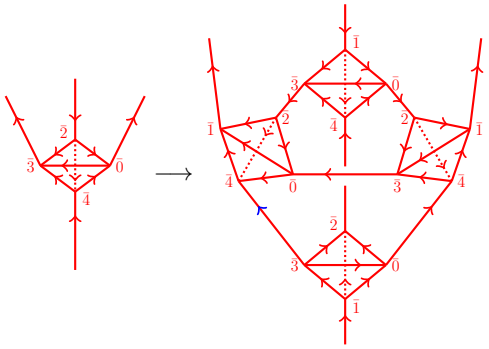

(b) For resolved dual lattice $\tilde{\mathcal{P}}$.

FIG. 31: (1-4)-B move.

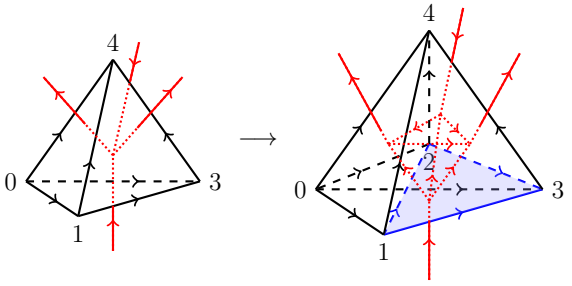

(a) For triangulation $\mathcal{T}$ and dual lattice $\mathcal{P}$.

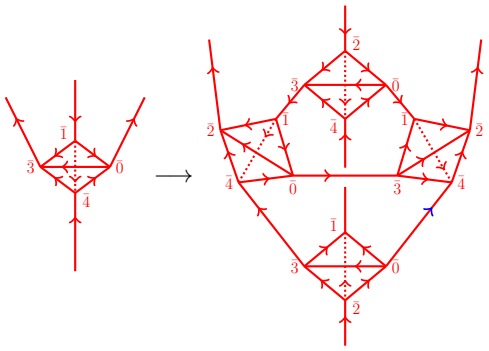

(b) For resolved dual lattice $\tilde{\mathcal{P}}$.

FIG. 32: (1-4)-C move.

out-leg string #	configuration #	configuration
0	1	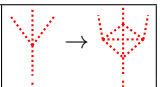
	4	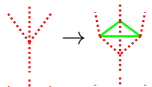
	3	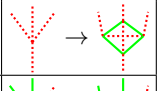
2	6×1	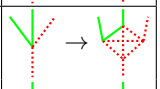
	6×2	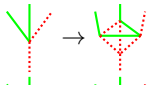
	6×2	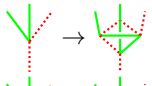
	6×2	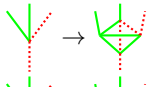
	6×1	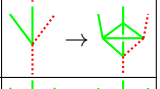
4	3	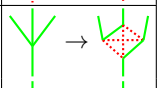
	4	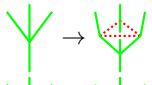
	1	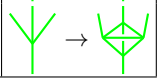

TABLE VI: $2^6 = 64$ kinds of configurations of Kitaev's Majorana chain decorations (green line) on the dual lattice $\mathcal{P}$ for each (1-4) move. The second column counts the number of configurations of the same symmetry type. When four green lines meet at one point, we should resolve the decoration according to the conventions in Fig. 18.

Appendix C: Abelian group structure of the general group super-cohomology solutions

Assume $(\nu_4, n_3, \tilde{n}_2)$ and $(\nu_4', n_3', \tilde{n}_2')$ are two solutions of the general group super-cohomology theory, i.e., they satisfy the equations

$$\mathrm{d}\nu_4 = \mathcal{O}[n_3, \tilde{n}_2], \tag{C1}$$
$$\mathrm{d}n_3 = \tilde{n}_2^2, \tag{C2}$$
$$\mathrm{d}\tilde{n}_2 = 0, \tag{C3}$$

and

$$\mathrm{d}\nu_4' = \mathcal{O}[n_3', \tilde{n}_2'], \tag{C4}$$
$$\mathrm{d}n_3' = \tilde{n}_2'^2, \tag{C5}$$
$$\mathrm{d}\tilde{n}_2' = 0. \tag{C6}$$

We want to construct another solution triple $(\nu_4^{\mathrm{tot}}, n_3^{\mathrm{tot}}, \tilde{n}_2^{\mathrm{tot}})$ from "adding" $(\nu_4, n_3, \tilde{n}_2)$ and $(\nu_4', n_3', \tilde{n}_2')$. The new solution satisfy

$$\mathrm{d}\nu_4^{\mathrm{tot}} = \mathcal{O}[n_3^{\mathrm{tot}}, \tilde{n}_2^{\mathrm{tot}}], \tag{C7}$$
$$\mathrm{d}n_3^{\mathrm{tot}} = (\tilde{n}_2^{\mathrm{tot}})^2, \tag{C8}$$
$$\mathrm{d}\tilde{n}_2^{\mathrm{tot}} = 0. \tag{C9}$$

If there exists such construction, then the solutions of the general group super-cohomology theory is closed under this "adding" and form an Abelian group (if the "adding" is commutative). The "adding" operation corresponds to stacking of two FSPT states physically.

The expressions of n_3^{tot} and $\tilde{n}_2^{\mathrm{tot}}$ are very simple. One can show that if we choose

$$n_3^{\mathrm{tot}} = n_3 + n_3' + \tilde{n}_2 \smile_1 \tilde{n}_2', \tag{C10}$$
$$\tilde{n}_2^{\mathrm{tot}} = \tilde{n}_2 + \tilde{n}_2', \tag{C11}$$

then Eqs. (C8) and (C9) can be derived from Eqs. (C2), (C3), (C5) and (C6).

Let us assume ν_4^{tot} has the expression

$$\nu_4^{\mathrm{tot}} = \nu_4 \cdot \nu_4' \cdot e^{i\pi\theta[n_3, n_3', \tilde{n}_2, \tilde{n}_2']}, \tag{C12}$$

where $\theta[n_3, n_3', \tilde{n}_2, \tilde{n}_2']$ is some unknown functional of $n_3, n_3', \tilde{n}_2, \tilde{n}_2'$. Since all of $n_3, n_3', \tilde{n}_2$ and $\tilde{n}_2'$ are cochains which are invariant under G_b action, so are $\theta[n_3, n_3', \tilde{n}_2, \tilde{n}_2']$ and ν_4^{tot}.

Denote the obstruction in Eq. (C1) by

$$\mathcal{O}[n_3, \tilde{n}_2] = (-1)^{n_3 \smile_1 n_3 + n_3 \smile_2 \mathrm{d}n_3 + f[\tilde{n}_2]}, \tag{C13}$$

where $\mathcal{O}_\gamma = (-1)^{f[\tilde{n}_2]}$ is the obstruction coming from the Majorana fermions. From Eqs. (C1), (C4) and (C7), the equation for θ is

$$\begin{aligned}(-1)^{\mathrm{d}\theta[n_3, n_3', \tilde{n}_2, \tilde{n}_2']} &= \frac{\mathrm{d}\nu_4^{\mathrm{tot}}}{\mathrm{d}\nu_4 \cdot \mathrm{d}\nu_4'} \\ &= (-1)^{(n_3^{\mathrm{tot}} \smile_1 n_3^{\mathrm{tot}} + n_3^{\mathrm{tot}} \smile_2 \mathrm{d}n_3^{\mathrm{tot}}) - (n_3 \smile_1 n_3 + n_3 \smile_2 \mathrm{d}n_3) - (n_3' \smile_1 n_3' + n_3' \smile_2 \mathrm{d}n_3') + f[\tilde{n}_2^{\mathrm{tot}}] - f[\tilde{n}_2] - f[\tilde{n}_2']}.\end{aligned} \tag{C14}$$

After substituting Eqs. (C10) and (C11) to the right hand side of the equation above, we obtain the (mod 2) linear equation

$$\begin{aligned}\mathrm{d}y[\tilde{n}_2, \tilde{n}_2'] \equiv\ & (\tilde{n}_2 \smile_1 \tilde{n}_2') \smile_1 (\tilde{n}_2 \smile_1 \tilde{n}_2') + (\tilde{n}_2 \smile_1 \tilde{n}_2') \smile_2 (\tilde{n}_2 \smile \tilde{n}_2' + \tilde{n}_2' \smile \tilde{n}_2) \\ & + (\tilde{n}_2^2 + \tilde{n}_2'^2) \smile_3 (\tilde{n}_2 \smile \tilde{n}_2' + \tilde{n}_2' \smile \tilde{n}_2) + \tilde{n}_2^2 \smile_3 \tilde{n}_2'^2 + f[\tilde{n}_2 + \tilde{n}_2'] - f[\tilde{n}_2] - f[\tilde{n}_2'], \pmod 2\end{aligned} \tag{C15}$$

where $y[\tilde{n}_2, \tilde{n}_2']$ is is related to $\theta[n_3, n_3', \tilde{n}_2, \tilde{n}_2']$ by

$$\theta[n_3, n_3', \tilde{n}_2, \tilde{n}_2'] = y[\tilde{n}_2, \tilde{n}_2'] + n_3 \smile_2 n_3' + (\tilde{n}_2 \smile_1 \tilde{n}_2') \smile_2 (n_3 + n_3') + (n_3 + n_3') \smile_3 (\tilde{n}_2 \smile \tilde{n}_2' + \tilde{n}_2' \smile \tilde{n}_2) + \tilde{n}_2^2 \smile_3 n_3'. \tag{C16}$$

In summary, if $y[\tilde{n}_2, \tilde{n}_2']$ is a solution of Eq. (C15), then the Abelian group structure of the group super-cohomology solutions is

$$(\nu_4, n_3, \tilde{n}_2) + (\nu_4', n_3', \tilde{n}_2') = (\nu_4 \nu_4' e^{i\pi\theta[n_3, n_3', \tilde{n}_2, \tilde{n}_2']}, n_3 + n_3' + \tilde{n}_2 \smile_1 \tilde{n}_2', \tilde{n}_2 + \tilde{n}_2'), \tag{C17}$$

where $\theta[n_3, n_3', \tilde{n}_2, \tilde{n}_2']$ is defined by Eq. (C16).

1. Explicit construction of $\theta[n_3, n_3', \tilde{n}_2, \tilde{n}_2']$

To construction $\theta[n_3, n_3', \tilde{n}_2, \tilde{n}_2']$ in the Eq. (C17), we only need to find a solution $y[\tilde{n}_2, \tilde{n}_2']$ of Eq. (C15). Note that, Eq. (C15) is a (mod 2) equation when evaluating for arbitrary $(g_0, g_1, g_2, g_3, g_4, g_5) \in G_b^6$. $y[\tilde{n}_2, \tilde{n}_2'](g_0, g_1, g_2, g_3, g_4)$ is automatically symmetric under G_b, for it depends on g_i through $\tilde{n}_2$ and $\tilde{n}_2'$.

As defined above, $y[\tilde{n}_2, \tilde{n}_2']$ is a functional of $\tilde{n}_2$ and $\tilde{n}_2'$. When evaluating at $(g_0, g_1, g_2, g_3, g_4)$, it is a function $y[\{\tilde{n}_2(g_i, g_j, g_k)\}, \{\tilde{n}_2'(g_i, g_j, g_k)\}]$ $(0 \le i < j < k \le 4)$. It seems that y has $2 \times C_5^3 = 20$ arguments. However, since $\tilde{n}_2$ is a cocycle with equation $\mathrm{d}\tilde{n}_2 = 0$ (mod 2), $\{\tilde{n}_2(g_i, g_j, g_k)\}$ $(0 \le i < j < k \le 4)$ are not fully independent. After solving the equations $\mathrm{d}n_2(g_i, g_j, g_k, g_l) = 0$ $(0 \le i < j < k < l \le 4)$ explicitly, we find that the number of independent cocycles $\tilde{n}_2(g_i, g_j, g_k)$ $(0 \le i < j < k \le 4)$ is 6. In fact, 2^6 is exactly the number of Kitaev chain decoration configurations of a 4-simplex, or a (2-3) Pachner move, see Table V. We can choose the 6 independent cocycles to be $\{\tilde{n}_2(012), \tilde{n}_2(013), \tilde{n}_2(014), \tilde{n}_2(023), \tilde{n}_2(024), \tilde{n}_2(034)\}$ [again, (012) means (g_0, g_1, g_2), etc]. The other 4 cocycles $\{\tilde{n}_2(123), \tilde{n}_2(124), \tilde{n}_2(134), \tilde{n}_2(234)\}$ can be derived from the previous 6 ones. Therefore, $y[\{\tilde{n}_2(g_i, g_j, g_k)\}, \{\tilde{n}_2'(g_i, g_j, g_k)\}]$ $(0 \le i < j < k \le 4)$ has only 12 independent arguments, and can be written as

$$y[\tilde{n}_2(012), \tilde{n}_2(013), \tilde{n}_2(014), \tilde{n}_2(023), \tilde{n}_2(024), \tilde{n}_2(034), \tilde{n}_2'(012), \tilde{n}_2'(013), \tilde{n}_2'(014), \tilde{n}_2'(023), \tilde{n}_2'(024), \tilde{n}_2'(034)]. \quad \text{(C18)}$$

Each $\tilde{n}_2$ or $\tilde{n}_2'$ can take two values, so the number of unknown variables of y is $q = 2^{12} = 4096$.

The number of equations in (C15) is the number of all possible cocycle $\tilde{n}_2$ and $\tilde{n}_2'$, i.e., the number of different cochain patterns $\tilde{n}_2$ and $\tilde{n}_2'$ satisfying $\mathrm{d}\tilde{n}_2(g_i, g_j, g_k, g_l) = \mathrm{d}\tilde{n}_2'(g_i, g_j, g_k, g_l) = 0$ $(0 \le i < j < k < l \le 5)$. One can solve the cocyle equation and find that the number of different $\tilde{n}_2(g_i, g_j, g_k)$ $(0 \le i < j < k \le 5)$ pattern is 2^{10}. This is the number of Kitaev chain decoration configurations of a 5-simplex, or the hexagon equation (see Fig. 21 for one configuration). So the number of equations is $p = 2^{20} = 1048576$.

The right hand side of Eq. (C15) involves $f(\tilde{n}_2)$. Because $\mathcal{O}_\gamma = (-1)^{f[\tilde{n}_2]}$ can be ± 1 or $\pm i$, $f(\tilde{n}_2)$ takes value in $\{0, \frac{1}{2}, 1, \frac{3}{2}\}$. To make the right hand side of Eq. (C15) integers, we can multiply Eq. (C15) by 2, and scale y by

$$y = \frac{x}{2}. \quad \text{(C19)}$$

The final equation for x in the matrix form is

$$Ax \equiv b, \quad \text{mod } 4. \quad \text{(C20)}$$

This is an overdetermined system of linear equations with $p = 2^{20}$ equations and $q = 2^{12}$ unknowns.

Using the procedure list in the next subsection, we find that the above linear equation indeed has solutions. We can use the solution x to construct θ. And the group structure of the general super-cohomology solutions is given by Eq. (C17).

2. Solving system of linear equations in $\mathbb{R}/4\mathbb{Z}$

In this subsection, we will discuss how to solve the equations of the form

$$Ax \equiv b, \quad \text{mod } 4. \quad \text{(C21)}$$

Here, $A \in M_{p,q}(\mathbb{Z})$ is a $p \times q$ $(p = 2^{20}, q = 2^{12})$ matrix with elements in $\mathbb{Z}$ (the matrix form of coboundary operator "d" has elements in $\mathbb{Z}$). On the right hand side, $b \in \mathbb{Z}^p$ is a $\mathbb{Z}$-valued vector with length p. However, $x \in \mathbb{R}^p$ is a $\mathbb{R}$-valued vector with length p. All the equations hold modulo 4. Note that this equation is not a system of linear equations in ring $\mathbb{Z}/4\mathbb{Z}$, for elements of x can take value in $\mathbb{R}/4\mathbb{Z}$, not merely $\mathbb{Z}/4\mathbb{Z}$. In fact, we find that the above equation in our case has no solution of x in $\mathbb{Z}/4\mathbb{Z}$, but has in $\mathbb{R}/4\mathbb{Z}$.

To solve the above (mod 4) equation, we introduce an integer variable n such that Eq. (C21) becomes an equation in $\mathbb{R}$ without modulo 4:

$$Ax = b + 4n. \quad \text{(C22)}$$

Now the equation holds in $\mathbb{R}$ and the unknowns are $x \in \mathbb{R}^p$ and $n \in \mathbb{Z}^p$.

The basic idea to solve Eq. (C22) is Gaussian elimination. Since x takes value in $\mathbb{R}$, we can use usual Gaussian elimination (column reduction) in field $\mathbb{R}$. However, for n takes value in $\mathbb{Z}$, the row reduction of Gaussian elimination can be only performed in ring $\mathbb{Z}$ (the invertible scalars are only ± 1). Performing Gaussian elimination in $\mathbb{Z}$ to solve

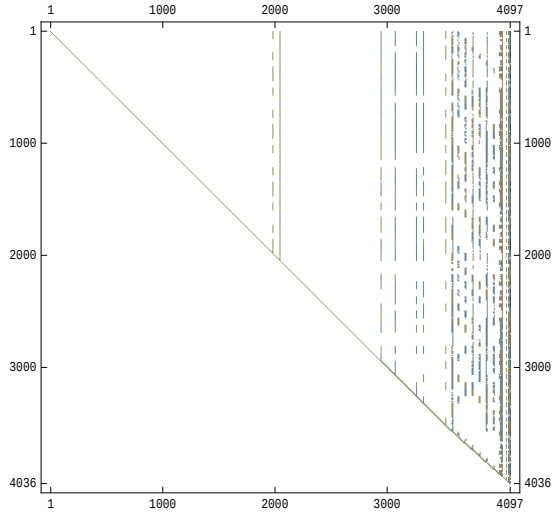

FIG. 33: Graphic display of the unique Hermite normal form of the augmented matrix (A, b). We omit all the zero rows below the nonzero ones (the number of zero rows is $p - r - 1 = 1044540$). White color represents zero matrix elements. The last element at $(r + 1, q + 1) = (4036, 4097)$ is 4, indicating the existence of solutions for Eq. (C20). The first nonzero element in each row of the Hermite normal form of A is either 1 or 2. So the Abelian group structure of the general group super-cohomology solutions takes value in $\mathbb{Z}_8$ rather than $\mathbb{Z}_4$.

linear equations is actually finding the Hermite normal form of A, which is the standard technique in solving system of linear Diophantine equations. The detailed procedures for solving Eq. (C22) are as follows.

We first find Hermite normal form of A:

$$UA = H, \tag{C23}$$

where $U \in M_{p,p}(\mathbb{Z})$ is a unimodular matrix with elements in $\mathbb{Z}$. H, as an upper triangular integer matrix, is the Hermite normal form of A. The equation becomes

$$Hx = b' + 4n' \tag{C24}$$

where

$$b' = Ub, \tag{C25}$$
$$n' = Un. \tag{C26}$$

Because U is a unimodular matrix which is invertible in $\mathbb{Z}$, we can construct a unique solution (x, n) of original equation Eq. (C22) from a solution (x, n') of the new equation Eq. (C24), and vice versa.

Now we perform column Gaussian elimination for H in $\mathbb{R}$, such that

$$HU = \begin{pmatrix} I_r & 0 \\ 0 & 0 \end{pmatrix}, \tag{C27}$$

where U is a invertible matrix in $\mathbb{R}$, and I_r is the identity matrix with size $r \times r$. The equation becomes

$$\begin{pmatrix} I_r & 0 \\ 0 & 0 \end{pmatrix} x' = b' + 4n' \tag{C28}$$

where

$$x' = U^{-1}x \tag{C29}$$

The solution of the new equation Eq. (C28) can be also used to construct a unique solution of Eq. (C24), for U is invertible in $\mathbb{R}$ (recall that x has elements in $\mathbb{R}$).

Eq. (C28) has solution (x', n') $(x' \in \mathbb{R}^p, n' \in \mathbb{Z}^p)$ if and only if the last $p - r$ elements of b' are all 0 (mod 4), i.e.,

$$b'_{p-r} \in (4\mathbb{Z})^{p-r}, \tag{C30}$$

where we have used notation $b' = \begin{pmatrix} b'_r \\ b'_{q-r} \end{pmatrix}$. If it is true, one can construct all the solutions of x' in Eq. (C28) and use them to obtain all x from Eq. (C29).

In summary, to know whether Eq. (C21) has solution (x, n) ($x \in \mathbb{R}^p, n \in \mathbb{Z}^p$) or not, we need to find the Hermite normal H of A ($UA = H$). Denote the number of nonzero rows of H by r. Then the next step is to check whether the last $p - r$ elements of Ub are all 0 (mod 4) or not. In practice, calculating the unimodular matrix U is very time consuming. We only need to find out the Hermite normal form of the augmented matrix (A, b). The original equation (C21) has solution if and only if the element in the $(r + 1)$-th row and $(q + 1)$-th column of the Hermite normal form is 0 (mod 4).

We used SageMath [74] to calculate the Hermite normal form of the augmented matrix (A, b) with size $p \times (q+1) = 2^{20} \times (2^{12}+1)$. The rank of A is found to be $r = 4035$, and the matrix element at the place $(r+1, q+1) = (4036, 4097)$ of the Hermite normal form is 4 (see Fig. 33). Therefore, the highly overdetermined Eq. (C20) indeed has solutions! We can use the solutions to construct the group structure of the general group super-cohomology solutions by Eq. (C17).

We further checked that the first nonzero element in each row of the Hermite normal form of A is either 1 or 2. So the solution x can be chosen to be in $\frac{1}{2}\mathbb{Z}$. And the phase factor $e^{i\pi\theta}$ in ν_4^{tot} takes values in $\mathbb{Z}_8 \cong \{e^{in\pi/4} | n \in \mathbb{Z}\}$. This implies that the cohomology operation defined by the obstruction is in fact in $\mathbb{Z}_8$ rather than $\mathbb{Z}_4$. This is a very interesting hierarchy structure: the obstruction in the special group super-cohomology has a $\mathbb{Z}_2$ phase factor which is the fermion sign, the Majorana fermion decoration gives a $\mathbb{Z}_4$ phase factor obstruction from Kitaev chain (p-wave superconductor), and the Abelian group structure of the general group super-cohomology theory takes value in $\mathbb{Z}_8$.

[1] Z.-C. Gu and X.-G. Wen, "Tensor-entanglement-filtering renormalization approach and symmetry-protected topological order," Phys. Rev. B **80**, 155131 (2009).

[2] Xie Chen, Zheng-Cheng Gu, Zheng-Xin Liu, and Xiao-Gang Wen, "Symmetry-protected topological orders in interacting bosonic systems," Science **338**, 1604–1606 (2012).

[3] X. Chen, Z.-C. Gu, Z.-X. Liu, and X.-G. Wen, "Symmetry protected topological orders and the group cohomology of their symmetry group," Phys. Rev. B **87**, 155114 (2013).

[4] M. Z. Hasan and C. L. Kane, "*Colloquium* : Topological insulators," Rev. Mod. Phys. **82**, 3045–3067 (2010).

[5] X.-L. Qi and S.-C. Zhang, "Topological insulators and superconductors," Rev. Mod. Phys. **83**, 1057–1110 (2011).

[6] Edward Witten, "Fermion path integrals and topological phases," Rev. Mod. Phys. **88**, 035001 (2016).

[7] F. D. M. Haldane, "Nonlinear field theory of large-spin heisenberg antiferromagnets: Semiclassically quantized solitons of the one-dimensional easy-axis néel state," Phys. Rev. Lett. **50**, 1153–1156 (1983).

[8] Xiao-Gang Wen, "Construction of bosonic symmetry-protected-trivial states and their topological invariants via $g \times so(\infty)$ nonlinear σ models," Phys. Rev. B **91**, 205101 (2015).

[9] A. Kapustin, "Symmetry Protected Topological Phases, Anomalies, and Cobordisms: Beyond Group Cohomology," ArXiv e-prints (2014), arXiv:1403.1467.

[10] M. Levin and Z.-C. Gu, "Braiding statistics approach to symmetry-protected topological phases," Phys. Rev. B **86**, 115109 (2012).

[11] Meng Cheng and Zheng-Cheng Gu, "Topological response theory of abelian symmetry-protected topological phases in two dimensions," Phys. Rev. Lett. **112**, 141602 (2014), arXiv:1302.4803.

[12] Chenjie Wang, Chien-Hung Lin, and Zheng-Cheng Gu, "Interacting fermionic symmetry-protected topological phases in two dimensions," arXiv e-prints (2016), arXiv:1610.08478.

[13] C. Wang and M. Levin, "Braiding statistics of loop excitations in three dimensions," Phys. Rev. Lett. **113**, 080403 (2014).

[14] S. Jiang, A. Mesaros, and Y. Ran, "Generalized modular transformations in $(3 + 1)$D topologically ordered phases and triple linking invariant of loop braiding," Phys. Rev. X **4**, 031048 (2014).

[15] C. Wang and M. Levin, "Topological invariants for gauge theories and symmetry-protected topological phases," Phys. Rev. B **91**, 165119 (2015).

[16] J. C. Wang and X.-G. Wen, "Non-abelian string and particle braiding in topological order: Modular $\mathrm{SL}(3, \mathbb{Z})$ representation and $(3 + 1)$-dimensional twisted gauge theory," Phys. Rev. B **91**, 035134 (2015).

[17] C.-H. Lin and M. Levin, "Loop braiding statistics in exactly soluble three-dimensional lattice models," Phys. Rev. B **92**, 035115 (2015).

[18] A. Vishwanath and T. Senthil, "Physics of three-dimensional bosonic topological insulators: Surface-deconfined criticality and quantized magnetoelectric effect," Phys. Rev. X **3**, 011016 (2013).

[19] C. Wang and T. Senthil, "Boson topological insulators: A window into highly entangled quantum phases," Phys. Rev. B **87**, 235122 (2013).

[20] X. Chen, F. J. Burnell, A. Vishwanath, and L. Fidkowski, "Anomalous symmetry fractionalization and surface topological order," Phys. Rev. X **5**, 041013 (2015).

[21] Chenjie Wang, Chien-Hung Lin, and Michael Levin, "Bulk-boundary correspondence for three-dimensional symmetry-protected topological phases," Phys. Rev. X **6**, 021015 (2016).

[22] P. Bonderson, C. Nayak, and X.-L. Qi, "A time-reversal invariant topological phase at the surface of a 3d topological insulator," Journal of Statistical Mechanics: Theory and Experiment **2013**, P09016 (2013).
[23] C. Wang, A. C. Potter, and T. Senthil, "Gapped symmetry preserving surface state for the electron topological insulator," Phys. Rev. B **88**, 115137 (2013).
[24] L. Fidkowski, X. Chen, and A. Vishwanath, "Non-abelian topological order on the surface of a 3d topological superconductor from an exactly solved model," Phys. Rev. X **3**, 041016 (2013).
[25] X. Chen, L. Fidkowski, and A. Vishwanath, "Symmetry enforced non-abelian topological order at the surface of a topological insulator," Phys. Rev. B **89**, 165132 (2014).
[26] C. Wang and T. Senthil, "Interacting fermionic topological insulators/superconductors in three dimensions," Phys. Rev. B **89**, 195124 (2014).
[27] M. A. Metlitski, C. L. Kane, and M. P. A. Fisher, "Symmetry-respecting topologically ordered surface phase of three-dimensional electron topological insulators," Phys. Rev. B **92**, 125111 (2015).
[28] Xie Chen, Zheng-Cheng Gu, and Xiao-Gang Wen, "Local unitary transformation, long-range quantum entanglement, wave function renormalization, and topological order," Phys. Rev. B **82**, 155138 (2010).
[29] K. Walker and Z. Wang, "(3+1)-tqfts and topological insulators," Front. Phys. **7**, 150 (2012).
[30] F. J. Burnell, X. Chen, L. Fidkowski, and A. Vishwanath, "Exactly soluble model of a three-dimensional symmetry-protected topological phase of bosons with surface topological order," Phys. Rev. B **90**, 245122 (2014).
[31] A. P. Schnyder, S. Ryu, A. Furusaki, and A. W. W. Ludwig, "Classification of topological insulators and superconductors in three spatial dimensions," Phys. Rev. B **78**, 195125 (2008).
[32] A. Kitaev, "Periodic table for topological insulators and superconductors," AIP Conference Proceedings **1134**, 22 (2009).
[33] Lukasz Fidkowski and Alexei Kitaev, "Effects of interactions on the topological classification of free fermion systems," Phys. Rev. B **81**, 134509 (2010).
[34] X.-L. Qi, "A new class of (2+1)-dimensional topological superconductors with $\mathbb{Z}_8$ topological classification," New Journal of Physics **15**, 065002 (2013).
[35] H. Yao and S. Ryu, "Interaction effect on topological classification of superconductors in two dimensions," Phys. Rev. B **88**, 064507 (2013).
[36] S. Ryu and S.-C. Zhang, "Interacting topological phases and modular invariance," Phys. Rev. B **85**, 245132 (2012).
[37] Z.-C. Gu and M. Levin, "Effect of interactions on two-dimensional fermionic symmetry-protected topological phases with Z_2 symmetry," Phys. Rev. B **89**, 201113 (2014).
[38] Yi-Zhuang You and Cenke Xu, "Symmetry-protected topological states of interacting fermions and bosons," Phys. Rev. B **90**, 245120 (2014).
[39] T. Morimoto, A. Furusaki, and C. Mudry, "Breakdown of the topological classification $\mathbb{Z}$ for gapped phases of noninteracting fermions by quartic interactions," Phys. Rev. B **92**, 125104 (2015).
[40] Chong Wang and T. Senthil, "Interacting fermionic topological insulators/superconductors in three dimensions," Phys. Rev. B **89**, 195124 (2014).
[41] C. Wang, A. C. Potter, and T. Senthil, "Classification of Interacting Electronic Topological Insulators in Three Dimensions," Science **343**, 629–631 (2014), arXiv:1306.3238.
[42] Zheng-Cheng Gu and Xiao-Gang Wen, "Symmetry-protected topological orders for interacting fermions: Fermionic topological nonlinear σ models and a special group supercohomology theory," Phys. Rev. B **90**, 115141 (2014).
[43] X. Chen, Z.-C. Gu, and X.-G. Wen, "Classification of gapped symmetric phases in one-dimensional spin systems," Phys. Rev. B **83**, 035107 (2011).
[44] L. Fidkowski and A. Kitaev, "Topological phases of fermions in one dimension," Phys. Rev. B **83**, 075103 (2011).
[45] A. Kapustin, R. Thorngren, A. Turzillo, and Z. Wang, "Fermionic Symmetry Protected Topological Phases and Cobordisms," arXiv e-prints (2014), arXiv:1406.7329.
[46] D. S. Freed, "Short-range entanglement and invertible field theories," arXiv e-prints (2014), arXiv:1406.7278.
[47] Davide Gaiotto and Anton Kapustin, "Spin tqfts and fermionic phases of matter," International Journal of Modern Physics A **31**, 1645044 (2016).
[48] L. Bhardwaj, D. Gaiotto, and A. Kapustin, "State sum constructions of spin-TFTs and string net constructions of fermionic phases of matter," ArXiv e-prints (2016), arXiv:1605.01640.
[49] M. Barkeshli, P. Bonderson, M. Cheng, and Z. Wang, "Symmetry, Defects, and Gauging of Topological Phases," ArXiv e-prints (2014), arXiv:1410.4540.
[50] M. Cheng, Z. Bi, Y.-Z. You, and Z.-C. Gu, "Towards a Complete Classification of Symmetry-Protected Phases for Interacting Fermions in Two Dimensions," arXiv e-prints (2015), arXiv:1501.01313.
[51] Chenjie Wang, "Braiding statistics and classification of two-dimensional charge-$2m$ superconductors," Phys. Rev. B **94**, 085130 (2016).
[52] T. Lan, L. Kong, and X.-G. Wen, "Classification of 2+1D topological orders and SPT orders for bosonic and fermionic systems with on-site symmetries," ArXiv e-prints (2016), arXiv:1602.05946.
[53] A Yu Kitaev, "Unpaired majorana fermions in quantum wires," Physics-Uspekhi **44**, 131 (2001).
[54] The fermion parity symmetry is gauged in such constructions.
[55] M. A. Metlitski, L. Fidkowski, X. Chen, and A. Vishwanath, "Interaction effects on 3D topological superconductors: surface topological order from vortex condensation, the 16 fold way and fermionic Kramers doublets," ArXiv e-prints (2014), arXiv:1406.3032.
[56] A. Kitaev, http://www.ipam.ucla.edu/abstract/?tid=12389&pcode=STQ2015.
[57] R. Queiroz, E. Khalaf, and A. Stern, "Classification of interacting fermionic phases by dimensional reduction," ArXiv

e-prints (2016), arXiv:1601.01596.
[58] Pavel Putrov, Juven Wang, and Shing-Tung Yau, "Braiding Statistics and Link Invariants of Bosonic/Fermionic Topological Quantum Matter in 2+1 and 3+1 dimensions," arXiv e-prints (2016), arXiv:1612.09298.
[59] M. Cheng, Z.-C. Gu, S. Jiang, and Y. Qi, "Exactly Solvable Models for Symmetry-Enriched Topological Phases," ArXiv e-prints (2016), arXiv:1606.08482.
[60] C. Heinrich, F. Burnell, L. Fidkowski, and M. Levin, "Symmetry enriched string-nets: Exactly solvable models for SET phases," ArXiv e-prints (2016), arXiv:1606.07816.
[61] Zheng-Cheng Gu, Zhenghan Wang, and Xiao-Gang Wen, "Classification of two-dimensional fermionic and bosonic topological orders," Phys. Rev. B **91**, 125149 (2015).
[62] P. W. Kasteleyn, "Dimer statistics and phase transitions," Journal of Mathematical Physics **4**, 287–293 (1963).
[63] David Cimasoni and Nicolai Reshetikhin, "Dimers on surface graphs and spin structures. i," Communications in Mathematical Physics **275**, 187–208 (2007).
[64] David Cimasoni and Nicolai Reshetikhin, "Dimers on Surface Graphs and Spin Structures. II," Communications in Mathematical Physics **281**, 445–468 (2008).
[65] Nicolas Tarantino and Lukasz Fidkowski, "Discrete spin structures and commuting projector models for two-dimensional fermionic symmetry-protected topological phases," Phys. Rev. B **94**, 115115 (2016).
[66] Brayden Ware, Jun Ho Son, Meng Cheng, Ryan V. Mishmash, Jason Alicea, and Bela Bauer, "Ising anyons in frustration-free majorana-dimer models," Phys. Rev. B **94**, 115127 (2016).
[67] Richard Z Goldstein and Edward C Turner, "A formula for Stiefel-Whitney homology classes," Proceedings of the American Mathematical Society **58**, 339–339 (1976).
[68] Note that the barycentric subdivision triangulation illustrated in Ref. 47 is a special case of this general construction of Stiefel-Whitney homology class [67].
[69] Udo Pachner, "P.l. homeomorphic manifolds are equivalent by elementary shellings," European Journal of Combinatorics **12**, 129 – 145 (1991).
[70] Francesco Costantino, "A calculus for branched spines of 3-manifolds," Mathematische Zeitschrift **251**, 427–442 (2005).
[71] If we choose the convention of pairing $\langle\bar{0}\bar{3}\rangle$ and $\langle\bar{1}\bar{2}\rangle$ of the four Majorana fermions at the center of tetrahedron $\langle 0123\rangle$, all the results are the same as the convention $\langle\bar{0}\bar{2}\rangle$ and $\langle\bar{1}\bar{3}\rangle$ used in main text of our paper. γ_{012A} and γ_{234B} can also be chosen consistently in the definition of X operators (see the discussion below Eq. (29)). The last choice of pairing $\langle\bar{0}\bar{1}\rangle$ and $\langle\bar{2}\bar{3}\rangle$ is different from the above two conventions, for the Majorana fermion parity is changed when four Kitaev string meet at one tetrahedron. However, we can shift the c fermion number $n_3(g_0, g_1, g_2, g_3)$ by one (mod 2) to absorb this fermion parity changes and then obtain the same obstruction results.
[72] N. E. Steenrod, "Products of cocycles and extensions of mappings," Annals of Mathematics **48**, 290–320 (1947).
[73] A. Kapustin and R. Thorngren, "Fermionic SPT phases in higher dimensions and bosonization," ArXiv e-prints (2017), arXiv:1701.08264 [cond-mat.str-el].
[74] The Sage Developers, *SageMath, the Sage Mathematics Software System (Version 7.3)* (2016), `http://www.sagemath.org`.